

## Review

## Recent advancements in carrier-selective contacts for high-efficiency crystalline silicon solar cells: Industrially evolving approach

K.-W.A. Chee <sup>a,b,\*</sup>, B.K. Ghosh <sup>c,d</sup>, I. Saad <sup>d</sup>, Y. Hong <sup>e</sup>, Q.H. Xia <sup>f</sup>, P. Gao <sup>g</sup>, J. Ye <sup>h</sup>, Z.J. Ding <sup>b</sup><sup>a</sup> BK21 Plus, Kyungpook National University, Daegu 41566, Korea<sup>b</sup> Hefei National Laboratory for Physical Sciences at Microscale, and Department of Physics, University of Science and Technology of China, Hefei 230026, China<sup>c</sup> Faculty of Engineering (Energy Research Unit), University Malaysia Sabah, Kota Kinabalu, Sabah 88400, Malaysia<sup>d</sup> Electrical and Electronic Engineering program, Faculty of Engineering, University Malaysia Sabah, Kota Kinabalu, Sabah 88400, Malaysia<sup>e</sup> Department of Chemical and Biochemical Engineering, College of Chemistry and Chemical Engineering, Xiamen University, Xiamen 361005, China<sup>f</sup> College of Information Science and Electronic Engineering, Zhejiang University, Hangzhou 310027, China<sup>g</sup> School of Materials, Sun Yat-sen University, Guangzhou 510275, China<sup>h</sup> Ningbo Institute of Materials Technology and Engineering, Chinese Academy of Sciences, Ningbo 315201, China

## ARTICLE INFO

## ABSTRACT

## Keywords:

Contact resistivity  
Surface passivation  
Carrier selectivity  
Charge transport  
Thermal stability  
Industrial firing

Carrier-selective crystalline silicon heterojunction (SHJ) solar cells have already reached superior lab-scale efficiencies. Besides judicious wafer thickness design, the optimal choice of passivation schemes and carrier-selective materials is essential for industry adoption. Appropriate reduction of process complexity and performance benefits through minimal recombination losses are key. Thus, along with well-designed back contacts, the development of low-temperature processable transparent passivating stacks that act as carrier-selective contacts (CSCs) is highlighted for their potential in circumventing the limited open-circuit photovoltage and contact-related losses in mainstream solar cells. In this review, effective passivation schemes deploying materials ranging from undoped metal oxides (MOs) to doped silicon are evaluated, with a focus on their significance for industrially viable passivating contact development. Passivation stack architectures with  $\text{SiO}_x$ /heavily doped polycrystalline silicon ( $n^+$ -/ $p^+$ -poly-Si) realize the most attractive polysilicon-on-oxide (POLO) junctions and related schemes, e.g., combined with tunnel oxide passivated contact (TOPCon) and interdigitated back contact (IBC) solar cells. It is envisioned that the industrial trend is to eventually shift from the p-Si passivating emitter rear contact (PERC) and passivated emitter and rear polysilicon (PERPoly), towards TOPCon architectures, due to high manufacturing yields and compatibility with large-area metal screen printing and alternative bifacial designs.

**Abbreviations:** TOPCon, Tunnel oxide passivated contact; SHJ, Silicon heterojunction; IBC-SHJ, Interdigitated back contact silicon heterojunction; c-Si, Crystalline silicon; a-Si:Hi, Intrinsic hydrogenated amorphous silicon; a-Si:Hp, P-type hydrogenated amorphous silicon; a-Si:Hn, N-type hydrogenated amorphous silicon; PERC, Passivating emitter rear contact; PERT, Passivated emitter rear totally diffused; PERPoly, Passivated emitter and rear polysilicon; BSF, Back surface field; CSCs, Carrier selective contacts; HIT, Heterojunction with intrinsic thin-layer;  $\text{SiO}_x$ , Silicon oxide; a-SiO<sub>x</sub>, Amorphous silicon oxide; a-SiO<sub>x</sub>In, Indium doped amorphous silicon oxide; SiN<sub>x</sub>, Silicon nitride; TiO<sub>x</sub>, Titanium oxide; MoO<sub>x</sub>, Molybdenum oxide; MO, Metal oxide; TMOs, Transition metal oxides; AZO, Al-doped ZnO; ITO, In-doped SnO<sub>2</sub>; ATO, Al-doped SnO<sub>2</sub>; FTO, F-doped SnO<sub>2</sub>; V<sub>oc</sub>, Open-circuit voltage; iV<sub>oc</sub>, Implied open-circuit voltage; FF, IFF; J<sub>SC</sub>, Fill factor; Implied fill factor, Short-circuit current density; D<sub>itb</sub>, Interface state density; J<sub>o</sub>, Recombination current density; ρ<sub>c</sub>, Contact resistivity; R<sub>MPP</sub>, Internal resistance at maximum power point; V<sub>MPP</sub>, Voltage at maximum power point; J<sub>MPP</sub>, Current density at maximum power point; DASH, Dopant-free asymmetric Si heterocontact; ECL, Electron-selective/collecting layer; HCL, Hole-selective/collecting layer; Poly-Si, Polycrystalline silicon; Fz-Si, Cz-Si; CVD, APCVD; PECDV, LPCVD; Float-zone silicon, Czochralski-grown silicon; Chemical vapor deposition, Atmospheric pressure chemical vapor deposition; Plasma-enhanced chemical vapor deposition, Low pressure chemical vapor deposition; TCOs, Transparent conductive oxides; TCDs, IL, Transparent conductive dielectrics; Interface layer, ALD, Atomic layer deposition; MIS, Metal-insulator-semiconductor; MS, Metal-semiconductor; FLP, Fermi level pinning; WF, Workfunction; FGA, Forming gas annealing; ISFH, Institute for Solar Energy Research GmbH; PHPS, Perhydropolysilazane.

\* Corresponding author at: BK21 Plus, Kyungpook National University, Daegu 41566, Korea.

E-mail address: [kvac2@cantab.net](mailto:kvac2@cantab.net) (K.-W.A. Chee).

## 1. Introduction

Solar energy is amongst the most important renewable energy resource to exploit towards sustainable energy conservation efforts, and especially promising is the low levelized cost of electricity comparable with that of fossil-fuel and on-shore wind-based technologies when adopting thin silicon wafers ( $< 160 \mu\text{m}$  thick) [1]. Photovoltaics that covert solar power into usable electricity are dominantly based on homojunction crystalline silicon (*c*-Si) technology featuring high-temperature diffused junctions, which occupy a worldwide market share in excess of 90%. From the traditional diffused homojunction and large-area metal-semiconductor contact through the more recent technologies, e.g., including back surface field (BSF) and passivated emitter rear contact (PERC) [2,3] key design challenges include tackling contact resistivity ( $\rho_c$ ) and surface recombination losses while focusing on economies of scale and low cost per watt of solar power generation. Whereas Al-BSF technology has been important for the success of the *c*-Si photovoltaics industry over the last decade, the limited power conversion efficiency (PCE  $\leq 20\%$ ) is mainly due to the high carrier recombination velocity at the rear surface [4,5]. Indeed, heavily doped emitter materials, which have either been diffused or deposited, have been used to realize carrier selectivity (see Fig. 1a), and enhance contact properties. Moreover, what has become a promising solution for the mainstream *c*-Si photovoltaics industry is the adoption of passivating contacts, also known as carrier-selective contacts (CSCs), which are thin films or stacks within the contact structure on the surface of the *c*-Si absorber that suppress surface carrier recombination and enhance charge carrier selectivity by providing a low contact resistivity to electrons (holes) while concomitantly impeding holes (electrons) (see Figs. 1b and 1c). Ensuring that the interfaces are well-passivated will significantly lessen recombination losses while the incorporation of functional materials for the transparent conductive oxide (TCO) layer and metallic contacts can enhance carrier collection and minimize resistive losses. In fact, CSCs formed by highly transparent electrodes are heralding a pivotal role in SHJ design that is industrially favored at present. Incorporating a passivating dielectric membrane between the Si rear side and Al contacts reduces the rear surface recombination losses, thus allowing up to  $\sim 24\%$ -efficient devices to be achieved in industrial PERC production [6]. Aluminum oxide ( $\text{Al}_2\text{O}_3$ ) is the most widely used passivation layer, featuring a high density of negative fixed charges ( $\sim 10^{13} \text{ cm}^{-2}$ ) that provides excellent and stable rear side passivation on p-type silicon (p-Si) [7,8]. However, PERC cells having diffused junctions and BSF yield PCEs that are chiefly bottlenecked by the high charge carrier recombination losses at the metal-Si contact regions [3,9]. Thus, the implementation of passivation and local contact strategies to ensure superb lateral conductivity is a complex technical problem involving the two-fold objectives of overcoming recombination losses and maintaining a low  $\rho_c$ . As an alternative to local metal contacts, dopant-free CSCs are deployed using full-area dielectric materials stacks [10], and advances in their industrial adoption succeeding PERC have recently been reported for next-generation photovoltaics production, attaining PCEs  $\geq 25\%$  [11]. There is also strong motivation towards reducing the active layer thickness of *c*-Si photovoltaics without significant bowing, coupled with the development of silicon heterojunction (SHJ) technologies incorporating doped CSCs that elevate the PCE above 26% [12].

The SHJ cell technology has existed for the past few decades, e.g., with the early commercial application of hydrogenated amorphous silicon (a-Si:H) layers pioneered by Sanyo Electric Company in 1980 [13], which then evolved into the heterojunction with intrinsic thin-layer (HIT) patented by Panasonic Inc. in 1991 [14], or that based on the polycrystalline silicon (poly-Si)/tunnel  $\text{SiO}_x$  layer passivated interdigitated back contact (IBC) by SunPower [15]. In the former structure, a stack of a-Si:H layers is deposited on both sides of the *c*-Si wafer (see Fig. 1b). An intrinsic a-Si:H (a-Si:H(i)) layer is critical to chemically passivate the *c*-Si surface, and a doped a-Si:H overlayer creates the p-n junction as well as to provide field-effect passivation using fixed charges.

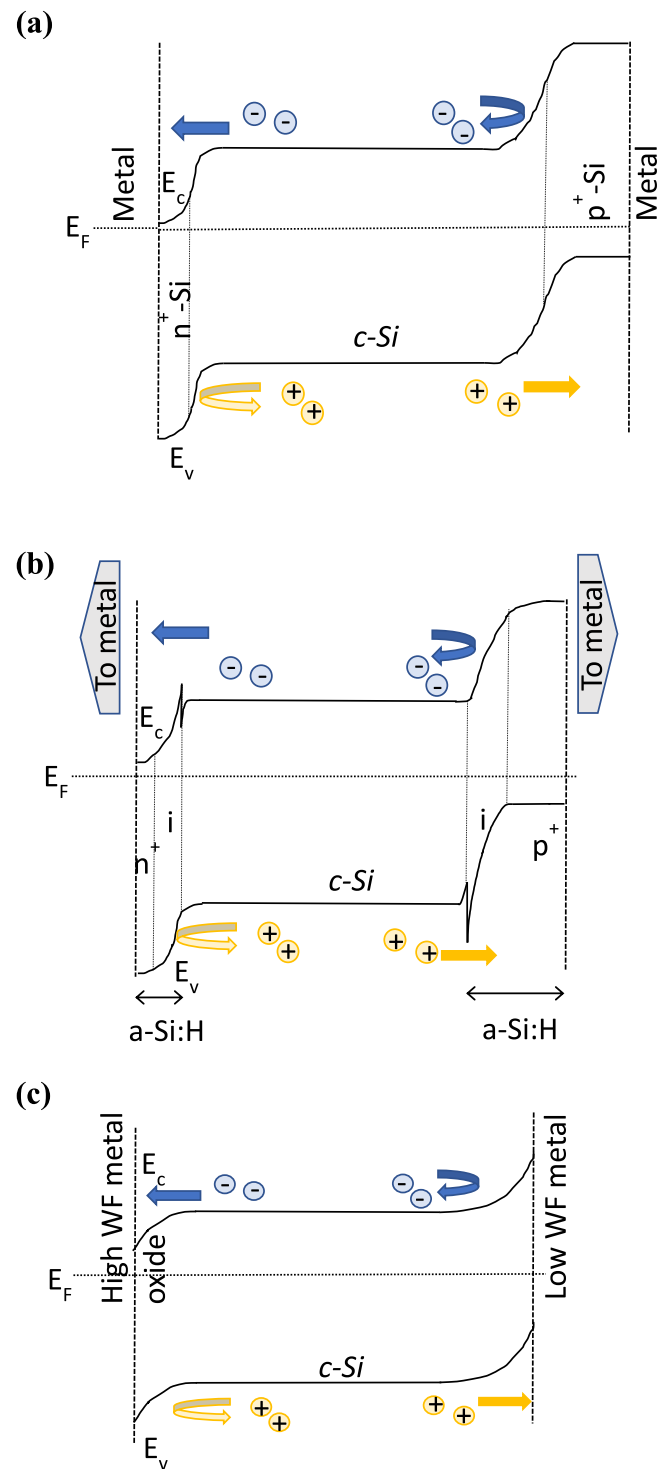


**Fig. 1.** Energy band diagrams illustrating general concepts of the idealized electron (hole) collecting layer/selective contact positioned at the far left (right) on an n-type *c*-Si wafer for (a) homojunction, (b) heterojunction, or (c) dopant-free asymmetric heterocontact, structure. Schematics are not drawn to scale.

On the front (illumination) side, the a-Si:H(i) passivation layer is followed by plasma-enhanced chemical vapor deposition (PECVD) or low pressure chemical vapor deposition (LPCVD) of a p-type a-Si:H (or a-Si:H (p)) emitter, and on the rear the a-Si:H(i) layer is followed by a BSF layer comprising an n-type a-Si:H (or a-Si:H(n)) film, and the doped a-Si:H films are capped with a stack of a TCO layer and a metallic contacting layer [16]. Nevertheless, while the doped a-Si:H deposition is often met

with process challenges, i.e., it might affect the properties of the ultra-thin a-Si:H(i) layers besides the stringent demands on the uniformity of film deposition across the cells, recent years have seen the PCE climb as high as 21.4% and 24.7/25.1%, respectively, for the p-type [17] and n-type [18,19] bifacial cells, and 26.6% for the n-type IBC architecture [12]. Compared with common high-efficiency silicon solar cell architectures such as that based on Al-BSF, PERC, or passivated emitter and rear totally diffused (PERT) structures, the n-type bifacial HIT was shown to exhibit the highest open-circuit voltage ( $V_{oc}$ ) value of 733 mV, and internal resistance at maximum power point (or voltage-to-current ratio at maximum power point,  $R_{MPP} = V_{MPP}/J_{MPP}$ ) of  $17.6 \Omega\text{cm}^2$  - a figure-of-merit that takes into account ohmic cell-to-module losses due to cell interconnections [20]. However, the doped a-Si:H film will also suffer from the intrinsic effects of free carrier absorption, doping-related Auger recombination, Shockley-Read-Hall recombination, and bandgap narrowing, which in turn adversely affect the device photovoltaic performance. Moreover, there are inherent limitations of requiring low-temperature processing, such as for metallization and interconnection. Therefore, while already affording excellent passivation properties, adopting alternative CSC designs is desirable.

Specifically, in place of an a-Si:H(i)/a-Si:H(n) stack in HIT cells, the polycrystalline silicon on oxide (POLO) contact architecture developed by Institute for Solar Energy Research GmbH (ISFH) is stable under high processing temperatures, which is based on an  $\text{SiO}_x$  passivation interface layer (IL) between the rear silicon surface and doped poly-Si contact layer. This temperature stability is compatible with mainstream high-temperature screen-print metallization [21]. Alternatively, tunnel oxide passivated contact (TOPCon) cells adopt ultrathin ( $\sim 1 \text{ nm}$ ) tunnel  $\text{SiO}_2/\text{n}^+$ -poly-Si at the rear contact region to attain full-area passivation, carrier selectivity, and low contact resistivity [22,23]. The rear side TOPCon and BSF design complement the screen-printed front surface passivating metal contact. 23%-efficiency was demonstrated on p-Si solar cells with full-area hole-selective passivating rear contact realized by a capping  $\text{SiO}_x$  layer on the doped poly-Si film, and also with phosphorous diffusion for the front side electron-selective contact together with a silicon nitride ( $\text{SiN}_x$ ) anti-reflection/passivation coating [24]. An even higher efficiency of 24.9% was achieved when implementing the back surface TOPCon on n-type silicon (n-Si) due to effective charge transport properties and concomittant selective conduction and surface passivation [25]. In particular, SHJ and TOPCon cells based on a-Si:H and  $\text{SiO}_x/\text{poly-Si}$ , respectively, have been expensive, but have great potential for production cost reductions, and presently, these approaches and hybrids are rigorously researched and could enter industry to compete with PERC on a cost-performance basis.

In SHJ cell production, the charge carrier selectivity of the electron (hole) collecting layer (or ECL/HCL) may also be achieved by deposited thin films of a different material that has a workfunction (WF) offset compared to that of the absorber material so that the potential difference at the absorber surface enables charge collection. In particular, very thin buffer dielectric layers are further inserted beneath the ECL/HCL for chemical passivation of the c-Si surface. Therefore, well-established industrially scalable thin-film deposition technologies are imperative for the maturity of the SHJ technology, which is well-suited for bifaciality, and has evolved greatly in terms of cost and efficiency. Fewer process steps are required compared to that of PERC, and the low-temperature processing is compatible with thinner wafers. Carrier selectivity can be achieved either by tunable WF metal oxide (MO) dielectrics or by doped poly-Si/a-Si:H. In the latter, the c-Si surface states will be passivated by hydrogenation, and there is no direct contact between the c-Si absorber and the metal, so that a high  $V_{oc}$  can be realized. However, to overcome the a-Si:H doping-related shortcomings and the huge production cost burden, dopant-free carrier-selective passivating contacts and hybrid heterojunction (HJ) technologies have recently emerged. Compared to mainstream technology, record-level efficiency solar cells combine the most successful HJs and field-passivated IBCs. Hybrid SHJ solar cells may adopt front side diffused contacts and rear

asymmetric CSCs. In addition to the simplicity of contact fabrication, the induced band-bending, electric field, and charge transport mechanisms, are important considerations for optimal photovoltaic performance. Not with standingly, dopant-free asymmetric heterocontact (DASH) silicon solar cells possess CSCs with superior passivation properties (see Fig. 1c) that leverage wide bandgap contact materials. In this approach, low-WF transition metal oxides (TMOs; e.g., titanium oxide ( $\text{TiO}_x$ ) [26,27] and zinc oxide ( $\text{ZnO}$ ) [28]), alkali or alkaline earth metal salts (e.g., lithium fluoride ( $\text{LiF}_x$ ) [27,29], magnesium fluoride ( $\text{MgF}_x$ ) [30], etc.), alkali or alkaline earth metal carbonates (e.g., cesium carbonate ( $\text{Cs}_2\text{C}_x\text{O}_y$ ) [31]) or transition metal (oxy)nitrides (e.g., tantalum nitride ( $\text{TaN}_x$ ) [32], titanium nitride ( $\text{TiN}$ ) [33], and titanium oxynitride ( $\text{TiO}_x\text{N}_y$ ) [34]), can be employed as ECLs. Organic interface dipoles can also be utilized to realize ultralow-WF electron-selective contact layers [35,36]. Among TMOs of high WF, molybdenum oxide ( $\text{MoO}_x$ ) [37–39] can serve very well as the hole-selective/collecting layer (HCL). In fact, SHJ solar cells with  $\text{MoO}_x$  and  $\text{TiO}_x$  as the hole- and electron-selective layers, respectively, on an n-Si wafer, were characterized as having a low temperature coefficient of the efficiency [40], thereby indicating effective mitigation of thermal losses. Efficiencies above 22% can be achieved (e.g., ref. [30, 40], etc.), with a high value reported so far of 22.1% [41] and 23.5% [38] for the electron-selective  $\text{TiO}_2$  and hole-selective  $\text{MoO}_x$  contacts, respectively, based on a full-area contact structure. When using  $\text{TiO}_2$ -based ECLs in a partial rear contact structure, efficiencies have reached as high as 24.1%, comparable to that using selective phosphorus-diffused emitters of state-of-the-art commercial cells [42]. In efficient DASH solar cells, surface accumulation is induced by a thin dielectric layer using fixed charges of opposite charge polarity [8]. The excess majority charge carriers at the surface assures field-effect passivation (or charge carrier population control) due to the high charge carrier asymmetry so that minority charge carrier diffusion occurs with minimal recombination losses at the interfaces. Efficient charge transport towards the contacts guarantees low electrical resistivity in the base region with dopant-free CSCs [8,43]. By moving the front contact grids to the rear of the device, front surface shadowing losses are avoided to achieve a high short-circuit current density ( $J_{sc}$ ) as in the case of the IBC design. IBC-SHJ solar cells are also equipped with effective field-effect passivation and optimal CSCs, earning the highest efficiencies of more than 25% [12,44]. However, IBCs are more difficult and expensive to fabricate, requiring the development of low-temperature metallization and interconnection procedures, as well as complex patterning strategies for the formation of interdigitated junctions. And from an industrially attractive standpoint, the highest efficiencies have also been maintained for silicon solar cells contacted on both sides, and adopting a full-area charge carrier-selective backside contact is necessary to preserve a potentially lean process sequence.

To summarize, Table 1 compares the state-of-the-art in the research and development of a range of silicon solar cell technologies, namely, those employing  $\text{MoO}_x$ - and  $\text{MgF}_x$ -based stacks as the HCL and ECL, respectively [30], with full-area back contacts featuring  $\text{MoO}_x$ - and  $\text{TiO}_x$ -based stacks as the HCL and ECL, respectively [40], or IBC designs with a-Si:H(n/p) rear passivating contact layers [12,44], monofacial DASH with MO-based passivation and ECL, monofacial [18,19] and bifacial [20] SHJ with a-Si:H(n/p) passivation, IBC-POLO [45,46], and TOPCon [24,25] structures. The industrial prospects for these solar cell technologies have also been reviewed [8,10,11,20]. However, the transition from Al-BSF to PERC architectures, and in the near future, possible industry alternatives to mainstream technology, remain elusive. Therefore, the prospects for HIT, POLO, hybrid IBC-SHJ, and TOPCon technologies, are broadly reviewed in terms of industrial development pathways toward ultimate sustainable design.

Due to their respective electron affinities and energy band offsets with the c-Si substrate, functional materials for the TCO and metal electrode can provide energy-barrier related electron and hole selectivity to constitute CSC performance, whereas a-Si:H dielectrics can obtain near-ideal asymmetric band offset by n-/p-type doping. Besides

**Table 1**

Photovoltaic performance records of various SHJ solar cells and their related architectures/technologies. A is active area and  $t_n$  ( $t_p$ ) is the n-(p)-type c-Si wafer thickness. FF is fill factor and PCE is power conversion efficiency.

Technology features and passivating scheme/materials	Wafer doping type and thickness	Performance levels	Ref.
Top/rear a-Si:H(i) passivation, with front side dielectric antireflective layer, and a-Si:H(n/p) rear side contact layers, $A = 180 \text{ cm}^2$ cell (IBC-HIT)	n-type; 165 $\mu\text{m}$	$V_{oc} = 0.744 \text{ V}$ , $J_{sc} = 42.3 \text{ mA/cm}^2$ , FF = 83.8, PCE = 26.3%	[12]
Top/rear a-Si:H(i) plus a-Si:H (n/p) contact layers, $A = 102 \text{ cm}^2$ cell (HIT)	n-type; 100 $\mu\text{m}$	$V_{oc} = 0.750 \text{ V}$ , $J_{sc} = 39.5 \text{ mA/cm}^2$ , FF = 83.0, PCE = 24.7%	[18]
Top/rear a-Si:H(i) plus a-Si:H (n/p) contact layers, $A = 152 \text{ cm}^2$ cell (HIT)	n-type; 160 $\mu\text{m}$	$V_{oc} = 0.738 \text{ V}$ , $J_{sc} = 40.8 \text{ mA/cm}^2$ , FF = 83.5, PCE = 25.1%	[19]
Top/rear a-Si:H(i) plus a-Si:H (n/p) contact layers, $A = 243 \text{ cm}^2$ cell (HIT)	n-type; 180 $\mu\text{m}$	$V_{oc} = 0.733$ , $J_{sc} = 37.3 \text{ mA/cm}^2$ , FF = 78.4, PCE = 21.5%	[20]
Top surface n-type doped emitter with passivation/antireflective layer and rear surface p-poly-Si/SiO <sub>x</sub> contact, $A = 4 \text{ cm}^2$ cell (TOPCon)	n-type; 180 $\mu\text{m}$	$V_{oc} = 0.701 \text{ V}$ , $J_{sc} = 41.1 \text{ mA/cm}^2$ , FF = 79.9, PCE = 23%	[24]
Top surface boron diffused emitter with Al <sub>2</sub> O <sub>3</sub> /SiN <sub>x</sub> passivation/antireflective layer and rear surface n-poly-Si/SiO <sub>x</sub> contact, $A = 4 \text{ cm}^2$ cell (TOPCon)	n-type; 180 $\mu\text{m}$	$V_{oc} = 0.718 \text{ V}$ , $J_{sc} = 42.1 \text{ mA/cm}^2$ , FF = 83.2, PCE = 25.1%	[25]
Top/rear a-Si:H(i) passivation, with SiN <sub>x</sub> :H/MgF <sub>x</sub> as top surface double layer antireflective coating, and MgF <sub>x</sub> /Al stack as top ECL and MoO <sub>x</sub> as bottom HCL, $A = 4.5 \text{ cm}^2$ cell (IBC-HIT)	n-type; 180 $\mu\text{m}$	$V_{oc} = 0.709 \text{ V}$ , $J_{sc} = 41.5 \text{ mA/cm}^2$ , FF = 75.6, PCE = 22.2%	[30]
Top/rear a-Si:H(i) passivation, with MoO <sub>x</sub> as top HCL and TiO <sub>x</sub> as rear ECL, $A = 4.5 \text{ cm}^2$ cell (HIT)	n-type; 180 $\mu\text{m}$	$V_{oc} = 0.723 \text{ V}$ , $J_{sc} = 39.2 \text{ mA/cm}^2$ , FF = 79.8, PCE = 22.6%	[40]
Top/rear a-Si:H(i) passivation, with front surface SiN antireflective layer, and TCO on a-Si:H(n/p) rear side contact layers, $A = 143.7 \text{ cm}^2$ cell (IBC-HIT)	n-type; 150 $\mu\text{m}$	$V_{oc} = 0.740$ , $J_{sc} = 41.8 \text{ mA/cm}^2$ , FF = 82.7, PCE = 25.6%	[44]
Top surface SiO <sub>x</sub> /SiN <sub>x</sub> /AlO <sub>x</sub> passivation/antireflective layer, and rear side i-poly-Si/SiO <sub>x</sub> and p-n/poly-Si/SiO <sub>x</sub> contact layers, $A = 9 \text{ cm}^2$ cell (IBC-POLO)	p-type; 300 $\mu\text{m}$	$V_{oc} = 0.727 \text{ V}$ , $J_{sc} = 42.62 \text{ mA/cm}^2$ , FF = 84.28, PCE = 26.1%	[45]
Top/rear a-Si:H(i) passivation, front side dielectric antireflective layer, and a-Si:H(n/p) rear side contact layers, $A = 180 \text{ cm}^2$ cell (IBC-HIT)	n-type; 200 $\mu\text{m}$	$V_{oc} = 0.740 \text{ V}$ , $J_{sc} = 42.5 \text{ mA/cm}^2$ , FF = 84.6, PCE = 26.6%	[47]
Top surface boron diffused emitter with PECVD-SiN <sub>x</sub> /thermal-MgF <sub>2</sub> passivation/antireflective layer and full-area n-poly-Si/SiO <sub>x</sub> passivating rear contact, $A = 4 \text{ cm}^2$ cell (TOPCon)	n-type; 200 $\mu\text{m}$	$V_{oc} = 0.724 \text{ V}$ , $J_{sc} = 42.8 \text{ mA/cm}^2$ , FF = 83.3, PCE = 25.8%	[48]

excellent charge carrier selectivity, the ECL/HCL has the potential to overcome intrinsic efficiency limitations choosing from a combination of chemical and field-effect passivation. Further, the doping of the poly-Si absorber surface below the unpassivated metal electrode endows ECL/HCL characteristics depending on the doping type. Among key

selection criteria are superior carrier selectivity, thermal stability, and contact resistivity. The high cost burden of PECVD or LPCVD, the use of flammable and pyrophoric silane, and toxic sources such as diborane and phosphine for doping, as well as parasitic absorption and limited lateral conduction, fundamentally constrain the industry incorporation of doped a-Si:H dielectrics in SHJ and POLO/TOPCon solar cells. Suitable alternatives to doped a-Si:H passivation to form CSCs may be represented by solutions that allow reduced active layer optical absorption, coupled with negligible  $\rho_c$ . Concurrently, there is much potential in employing undoped sub-stoichiometric MOs, as much as n-/p-type doped poly-Si, to lower CSC losses.

Dielectric stack passivation is a widely preferred strategy to improve the effective minority carrier lifetime ( $\tau_{eff}$ ), implied open-circuit voltage ( $iV_{oc}$ ), and efficiency. Reduced recombination current densities ( $J_o$ ), and improved carrier-selectivity performance have been linked to the superior passivation properties of the dielectric stack. MOs or doped poly-Si can also minimize  $\rho_c$ , thus providing two-fold benefits. Furthermore, cost-effective TCOs can play a vital role in the solar cell structure along with the dielectric stack, guaranteeing maximum light coupling into the c-Si absorber and efficient lateral charge transport to the contacts, as well as ensuring a low contact resistance. The adoption of highly transparent and electrically conductive materials combined with dielectric stacks for surface passivation and carrier-selective purposes, fit well into the industrial framework and feature a commitment to low optical losses, a highly competitive  $J_{sc}$ ,  $V_{oc}$ , and efficiency, by integrating advanced CSC strategies with mainstream processes for c-Si solar cell technologies. Importantly, the physical properties of nanostructure passivating materials, such as the thickness and dielectric constant, bear significant influence on the surface energy band structure or interfacial electric fields to induce charge accumulation or deplete charges at the surface. The built-in field is considered beneficial to improve charge carrier transport and suppress recombination losses during lateral conduction *en route* to the respective contacts [12,30],[40,43,44]. Through Eq. 1, it can be seen that the effective charge modulation at the surface is directly proportional to the dielectric constant of the nanostructure passivation layer. Therefore, for efficient electrical passivation, high-k dielectrics are highly effective passivation layers, as according to:

$$Q_{eff} \propto \frac{\epsilon A}{d} \quad (1)$$

where  $Q_{eff}$  is effective charge density,  $\epsilon$  is dielectric permittivity,  $d$  is thickness, and  $A$  is area.

Structural parameters such as the ratio of the contact area to passivation area, and the physical properties of the passivation material stack, have a tremendous influence on charge carrier selectivity. These parameters have been carefully accounted for together with CSCs with or without doping, through industry technology evolution from metal BSF to PERC, HIT, POLO, IBC-SHJ and TOPCon. The built-in field formed by the dielectric passivation layer has a crucial effect on the substrate-dielectric interface passivation. Population control of the charge carriers is determined by this built-in field at the hetero-interface, which in turn governs  $J_o$ . From an industrial standpoint similar to that for mainstream Al-BSF and PERC technologies, doping of the a-Si:H passivation layer in the HIT-based solar cell is necessary to form an ohmic contact. Commonly employed transparent conductive dielectrics (TCDs) such as SiN<sub>x</sub>, AlO<sub>x</sub> and SiO<sub>x</sub> sub-stoichiometric IL passivating thin films, are typically combined with a-Si:H passivation for high-efficiency c-Si solar cells. Surface passivation with SiN<sub>x</sub> and Al<sub>2</sub>O<sub>3</sub> for n- and p-Si wafers, respectively, have been reported to be vital to establish charge carrier asymmetry to enhance electrical conduction - a principle which is also equally applicable to p- or n-type a-Si:H [8]. Such passivation stacks are not only required to induce charge accumulation (majority carriers) but also charge inversion (minority carriers), at the surface.

## 2. Significance of carrier-selective and dopant-free materials

With industry-proven Al-BSF and PERC, the use of passivation layers is preferred that are highly transparent and electrically conductive, and also allow low carrier recombination and contact resistivity losses. Amongst the various c-Si solar cell technology pathways displayed in Table 1, low-temperature ( $< 200$  °C) deposition and processing of dopant-free CSCs are far less complex compared to that for doped passivation layers. In fact, n-Si wafers are highly favored for industrial manufacturing processes because of the greater tolerance to common metal contaminants and induced/introduced defects [49,50]. Hence, compared to p-Si substrates, n-type float-zone (Fz)-Si or even Czochralski-grown (Cz)-Si possesses superior minority carrier diffusion lengths so that bulk recombination losses are smaller. Moreover, the avoidance of considerable light-induced degradation is an advantage, unlike for p-type Cz-Si due to boron-oxygen pairs [51,52]. While doped a-Si:H dielectrics have been important for efficiency enhancement in all SHJ technologies, two major drawbacks have been identified that need to be addressed for front contact-related opto-electrical loss mitigation: 1) the relatively small bandgap of doped a-Si:H leads to greater parasitic absorption losses, and the 2) toxic material/doping sources which can sometimes be costly. Thus, the motivation arises to employ relatively cheap dopant-free CSCs having superior optical transparency on both sides of the c-Si wafer. As an example, the  $\text{SiN}_x/\text{Al}_2\text{O}_3$  dielectric stack in the diffused junction solar cell structure operates with a similar mechanism as that of the a-Si:H surface layer in the SHJ solar cell. Besides, the parasitic absorption loss in  $\text{SiN}_x$  and  $\text{Al}_2\text{O}_3$  dielectrics pales in comparison to that in doped a-Si:H dielectrics. When forming passivation contacts from atomic layer deposition (ALD), such as ALD- $\text{Al}_2\text{O}_3$  for localized back contact passivation, metal diffusion or electron trapping due to impurities found in mainstream p-Si solar cell processes, are averted [7,8]. Compared to using the Al contact in the metal-insulator-semiconductor (MIS) structure, ALD- $\text{Al}_2\text{O}_3$  provides long-term stability in combining both electrical and chemical passivation within PERC architectures.

Large-area passivation at the  $\text{SiO}_x/\text{poly-Si}$  interface is promising for back contacts in the TOPCon architecture [24,25,53,54]. Significantly, optical losses in ALD- $\text{Al}_2\text{O}_3$  are smaller compared to those in ALD- $\text{SiO}_x$ . Due to the wider band gaps of ALD- $\text{Al}_2\text{O}_3$  and  $\text{SiO}_2$ , electrical conduction to the contacts is supported by quantum-mechanical tunneling, thus ensuring their suitability for large-area solar cells. Optical transparency and carrier-selective properties, along with affordable surface passivation, are important features of TCDs that render them vast research and practical application areas of interest as dopant-free CSCs. While doped a-Si:H passivation layers may be highly effective, parasitic absorption losses are very significant in contrast to dopant-free CSCs. Furthermore, in a diffused junction a high doping concentration is needed to overcome strong interface-related Fermi level pinning (FLP). Otherwise, dopant-free CSCs are essential to combat FLP effects [8,30,43,40,55,56] through sensible selection of the material WF with respect to the wafer doping level on which  $\rho_c$  is highly dependent. As shown in Eq. 2,  $\rho_c$  is related to the Schottky barrier height  $\varphi_B$  and the bulk doping density  $N_d$  through:

$$\rho_c \propto \exp\left(\frac{\varphi_B}{\sqrt{N_d}}\right) \quad (2)$$

From a technological perspective, the approach relying on n-type bulk doping to reduce the contact resistance is challenging, because of the introduction of doping-related defects that will result in considerable bulk resistivity losses [19]. Additionally, the thermal budget required for dopant activation and diffusion is high, which has therefore persuaded photovoltaics research into the direction of dopant-free CSC development for n-Si solar cells.

The selection and extraction of free charge carriers can be managed without the doping approach since the same mechanism can be

accomplished by using the energy band offset due to the material WF. An adequately high or low WF can sustain either an accumulation or inversion regime at the surface under illumination, thus resulting in asymmetric electron or hole conduction. This contact strategy was initiated a few years ago as a cost-effective design, but recent advancements in industrial processes and guidelines to realize CSC production pathways have made it ever more attractive [57]. For example, low-temperature processed dopant-free  $\text{MoO}_x$ -based HCLs offer a greater performance-to-cost ratio when combined with a low-WF compound such as sub-stoichiometric  $\text{TiO}_x$  [26,57,58],  $\text{MgF}_x$  [59],  $\text{MgO}_x$  [60], and  $\text{LiF}_x$  [29], to serve as the ECL to minimize surface recombination- and  $\rho_c$ -related losses. For further lowering of the contact resistance and to alleviate FLP effects for enhanced passivation, the use of elemental extremely-low-WF alkaline earth metal/post-transition metal candidates such as Mg, Ca, or Al, is generally very attractive for back contact fabrication on n-type c-Si solar cells.

Inspired by hybrid organic-inorganic electronics, organic films, such as those based on Spiro-OMeTAD [61], TAPC [62], and PEDOT:PSS [63], have been investigated for hole-selective contacts on planar c-Si substrates. Otherwise, as have been researched for organic solar cells [64], high-WF ( $> 5$  eV) TMO materials such as  $\text{MoO}_x$  [55,65,66],  $\text{WO}_x$  [55,65,66],  $\text{NiO}_x$  [67], and  $\text{VO}_x/\text{V}_2\text{O}_x$  [65,66,68–71] are most promising due to the similar requisites for organic and inorganic absorbers not only to serve as the HCL for SHJ cells [72,73], but also for organic-inorganic perovskite solar cells [74]. Fig. 2 shows the metal (oxide/salt) IL thickness dependence of the contact resistance, with minimal values expected for thinner layers in general. Usually, the effect of oxygen vacancies is to modify the energy band structure and bandgap of TMOs to render them as n-type dielectrics. Nevertheless, Battaglia et al. [75] described a novel approach of using  $\text{MoO}_x$  as the hole-selective p-emitter for n-Si photovoltaics. On the other hand,  $\text{MoO}_x$  has also been successfully employed for p-Si photovoltaics as the hole collecting contact (p-BSF) [37]. Thus,  $\text{MoO}_x$  can be implemented to collect holes in both n- and p-type c-Si absorbers. However, charge carrier injection and recombination at defect sites are known to affect electrical transport properties. Afterwards, Bullock et al. [76] investigated  $\text{LiF}_x$  and  $\text{MoO}_x$ , respectively, for electron- and hole-selective asymmetric heterocontacts, together with a-Si:H(i) membrane passivation on both sides of the SHJ solar cell. The band-bending near the  $\text{MoO}_x/c\text{-Si}$  interface and the  $\text{Al}/\text{LiF}_x/c\text{-Si}$  interface play an important role in maintaining high  $V_{oc}$  and high FFs [77]. Interfacial contact passivation was shown to be paramount in suppressing electrical performance losses. In this approach, an even thinner ( $< 50$  nm) sub-stoichiometric  $\text{MoO}_x$  or  $\text{LiF}_x$  layer was adopted to realize the dopant-free hole- or electron-selective contact, respectively, to achieve decently high efficiencies. The high-WF TMOs afford superior carrier-selectivity, but its impact on the energy band structure-related degradation of photovoltaic parameters will be reported later.

### 2.1. Implications in using $\text{TiO}_x$ in CSCs

MIS-based passivating contacts with targeted low contact resistance emerged in the past to surpass traditional metal-semiconductor (MS) contact performance blighted by significant recombination losses. Nevertheless, advanced passivating contacts, also known as heterocontacts, are new industrially-favored technologies. The back contact losses related to the c-Si solar cell are crucial factors accounting for the decline in  $V_{oc}$  and efficiency [57,75]. In terms of reducing back contact recombination losses as well as increasing the electron-selectivity and hole-blocking capabilities in which the relative barrier height is essential, better potential was shown for the TMO (e.g.,  $\text{TiO}_2$ )/p-Si than for the Al/p-Si Schottky diode [78]. The low barrier height for electrons and large barrier height for holes allow effective electron conduction, and the simultaneous back contact passivation facilitates majority carrier transport by diffusion in n-type SHJ solar cells. The one-diode current equation after Shockley's theory shows the dependence on temperature

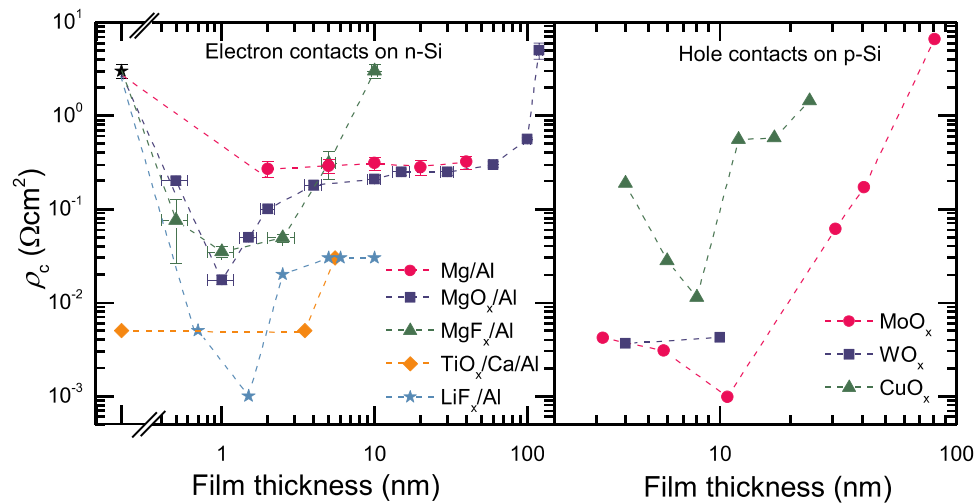


**Fig. 2.** Contact resistivity ( $\rho_c$ ) for various electron- and hole-selective contacts as a function of film stack thickness of the low-WF metal (oxide)/alkali and alkaline earth metal fluorides, or high-WF TMO. (used with permission from [8]).

$T$  and barrier height,  $\varphi_B$ :

$$I = I_s \exp \left[ \left( \frac{e(V + IR_s)}{\eta k_B T} \right) - 1 \right] \quad (3)$$

where  $\eta$  is the ideality factor,  $k_B$  is the Boltzmann constant,  $R_s$  is series resistance, and the prefactor  $I_s$  is the dark saturation current expressed as:

$$I_s = AA^*T^2 \exp \left( -\frac{q\varphi_B}{kT} \right) \quad (4)$$

where  $A$  is the contact area and  $A^*$  is the Richardson constant.

Whereas the material WF or  $\rho_c$  is determined by the active dopant concentration, carrier selectivity is dictated by the energy band offset. The thin  $\text{TiO}_x$  layer allows high optical transparency while majority carrier conduction is governed by the thermionic emission process over the low barrier height. Thus, common passivating materials, such as ultra-thin sub-stoichiometric  $\text{SiO}_x$ ,  $\text{TiO}_x$ , and  $\text{AlO}_x$  are usually employed as dopant-free carrier-selective TCDs. Basically, highly stable and carrier-selective dopant-free  $\text{TiO}_x$ -based contacts have been widely reported in the literature allowing conversion efficiencies of at least 20% [26,41,42,57,58,79,80]. Characteristically, the introduction of an  $\text{TiO}_x$  IL at the a-Si:H(i)/low-WF metal interface will harness the superior quality chemical passivation of a-Si:H(i) but increases  $\rho_c$  due to the inherent poor conductivity, which in turn likely limited the corresponding cell efficiencies previously reported to approximately 15% or less [81]; if surface passivation were prioritized over  $\rho_c$ , a thicker  $\text{TiO}_x$  film will be applied, and vice versa [80,82]. According to Cho et al. [83], the incorporation of ALD- $\text{TiO}_x$  in the a-Si:H(i)/ $\text{TiO}_x$ /low-WF metal contact structure effectively attained high quality passivation and a low  $\rho_c$  leading to an 18.2% efficient device, thus substituting for the requirement of a heavily doped a-Si:H layer. The thermal and environmental stability of  $\text{TiO}_x$ -based contacts is also well known [79,84]. Yang et al. [80] showed that on the rear surface of the n-Si wafer, sub-stoichiometric ALD- $\text{TiO}_x$  (~4.5 nm thick) in a full-area contact structure provided superior surface passivation (maximum effective surface recombination velocity reduced from a value of  $10^6$ – $10^7$  cm/s to 56 cm/s) and lower  $\rho_c$  (reduced from 0.5 to  $1.0 \Omega \cdot \text{cm}^2$  to a minimum value of  $\sim 20 \text{ m}\Omega \cdot \text{cm}^2$ ) after annealing compared to that of direct Al/n-Si contacts; and with a barrier height formed for holes due to a large valence band offset ( $\Delta E_v \sim 2.0$  eV) and excellent electron selectivity and extraction arising from a small conduction band offset ( $\Delta E_v \sim 0.05$  eV), ultimately enabled an efficiency of 19.8%. Enhancement in the

passivation thermal stability of the  $\text{TiO}_2$  film on the n-Si surface was elicited by the additional insertion of a thermally grown tunnel  $\text{SiO}_2$  layer (~1.2 nm thick) between the c-Si and  $\text{TiO}_2$  film, so that the maximum effective surface recombination velocity further reduced to 14 cm/s after annealing, thereby increasing the efficiency to 21.6%. Reproducibility of the c-Si solar cells with full-area  $\text{SiO}_2/\text{TiO}_2$  ECL was illustrated with an average efficiency above 21.0% [80]. The main process sequence for the fabrication of n-Si solar cells featuring a full-area rear  $\text{TiO}_2$  contact is shown in Fig. 3.

Other notable MO semiconductors that have also been investigated as ECL materials mainly due to ease of processing and low-cost fabrication include  $\text{ZnO}$  [28],  $\text{SnO}_2$  [85,86],  $\text{MgO}$  [60], and  $\text{TaO}_x$  [87]. However, although  $\text{ZnO}$  may offer the highest electron mobility amongst the present options, stability issues tend to affect device performance.  $\text{SnO}_2$  may offer better stability than  $\text{ZnO}$  and demonstrate significant reduction of barrier height and passivation of the silicon surface [85], but low  $\rho_c$ , and excellent surface passivation and high electron extraction efficiency have not been adequately achieved without further processing. While stability issues may be suppressed, efficiencies attained using  $\text{MgO}$  and  $\text{TaO}_x$  have not broken through the 20%-efficiency mark so far (i.e., for cells without the a-Si:H membrane). Nevertheless, the  $\text{TiO}_2$ -based film, i.e., with a tunnel- $\text{SiO}_2$  layer inserted between the c-Si and dopant-free contact layer to improve surface passivation, stably withstands industry-standard quick firing conditions so that with further optimization, the adoption of full-area  $\text{TiO}_2$ -based ECL allowed more than 22%-efficiency within the following year (see Fig. 4) [41]. For these reasons,  $\text{TiO}_x$  is by far most commonly employed for ECLs at present. The progression from using single-layer  $\text{TiO}_x$  film [26] to bilayer  $\text{SiO}_2/\text{TiO}_x$  for back contact passivation [41,80] reduces  $J_0$  and  $\rho_c$  remarkably. The conversion efficiency and architecture evolution of c-Si solar cells with full-area electron-selective  $\text{TiO}_2$  contacts (without the a-Si:H layer) are shown in Fig. 4. Hence, the dopant-free CSC derived from  $\text{TiO}_x$  is a facile alternative to the heavily doped silicon contact layer-based SHJ or POLO/TOPCon technologies. Furthermore, cell geometry and process iterations for an Al/LiFx/TiOx (minimum  $\rho_c < 40 \text{ m}\Omega \cdot \text{cm}^2$ ) or Al/TiOx/SiOy (minimum  $\rho_c \sim 50 \text{ m}\Omega \cdot \text{cm}^2$ ) partial rear contact stack have led to a record-level efficiency as high as 23.1% [88] or 24.1% [42], respectively, within the family of  $\text{TiO}_x$ -based electron selective heterocontacts on n-Si wafers.

## 2.2. The significance of TCOs for CSCs

Advanced passivation design schemes applied in mainstream CSC

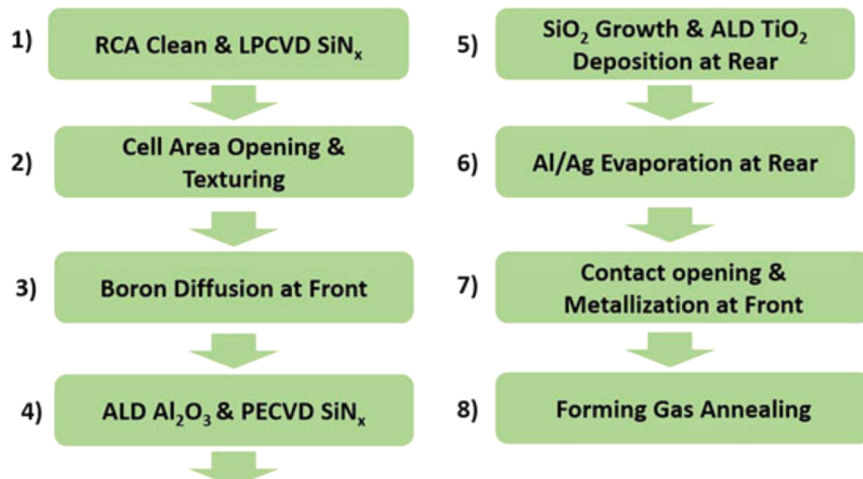


**Fig. 3.** Main process sequence for fabrication on n-Si solar cells with a full-area TiO<sub>2</sub> contact at the rear.  
(used with permission from [41]).

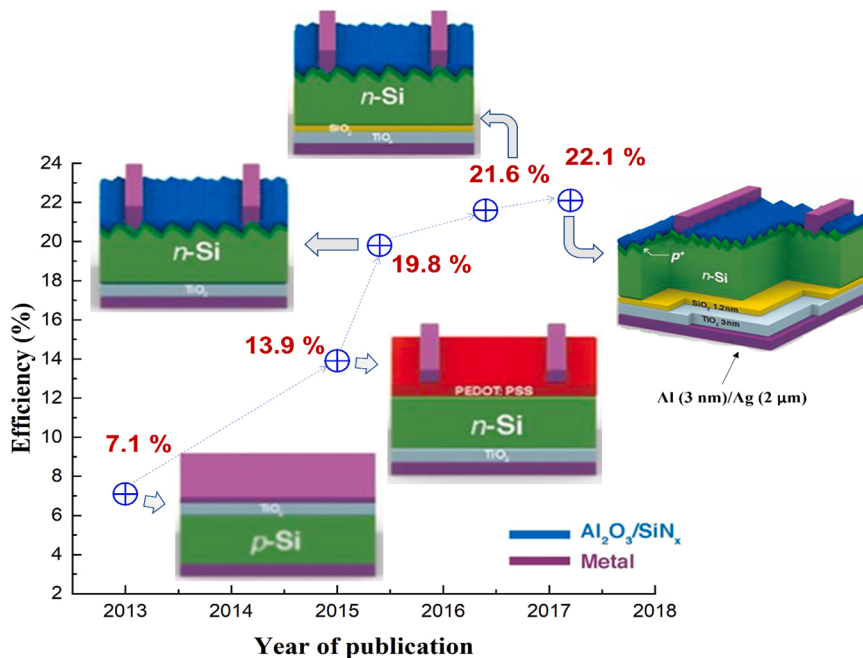


**Fig. 4.** Conversion efficiency and structure evolution of silicon solar cells with full-area electron-selective contacts.  
(adapted from [41])

technologies, such as HIT cells, consist of the room-temperature sputter deposition of the TCO layer to cater for the lateral transport of charge carriers to the metal grid, and to ensure maximum light coupling into the silicon substrate. The most efficient SHJ technologies make use of a-Si:H (i) plus doped a-Si:H thin films to allow extremely low surface recombination and effective carrier-selective collection, and this is capped with a TCO layer for enhanced lateral conductivity. Hence, within industrial frameworks, there is a prevalent need in the fabrication of carrier-selective TCOs. Commonly used wide bandgap TCO materials are doped CdO, Al-doped ZnO (AZO), In-doped SnO<sub>2</sub> (ITO), Al-doped SnO<sub>2</sub> (ATO), Ga-doped ZnO (GZO), and F-doped SnO<sub>2</sub> (FTO), offering n-type electrical conduction. At present, AZO and GZO are promising alternatives to ITO for thin film transparent electrode applications, with the best candidate being AZO having a low resistivity of the order of  $10^{-4}$  Ω-cm, and stemming from inexpensive and non-toxic source materials [89]. While p-type TCOs such as NiO, CuGaO<sub>2</sub>, Mg-doped ZnO, N-doped

ZnO, In-doped ZnO, etc., [90] would find applications as hole-transport layers, they are less common due to stability issues [89] as well as inferior electrical properties arising from the lower carrier mobility with values typically less than  $5 \text{ cm}^2 \text{V}^{-1} \text{s}^{-1}$ .

The key features of the high-performance thin TCO film include a  $\rho_c$  value as low as  $< 10^{-5}$  Ω-cm and optical transparency as high as  $> 90\%$  [91], but accompanied by a need to negotiate a trade-off relationship for specific applications. For example, to reduce parasitic absorption, a low free carrier concentration is a necessary condition, but this in turn increases the electrical resistivity. Moreover, the degenerate doping of the TCO film easily allows a low-resistivity ohmic contact with the metal grid. Doping of the TCO should, therefore, be carefully managed to maintain excellent charge carrier transport properties [89]. The low extinction coefficient,  $k$ , in the visible waveband allows high optical transparency. Furthermore, the sheet resistance,  $R_s$ , of the TCO layer, is related to its thickness  $d$  and conductivity  $\sigma$  through:

$$R_s = \frac{1}{\sigma d} \quad (5)$$

Hence, while increasing the doping concentration [92] or TCO layer thickness can lower  $\rho_c$  and promote electrical conductivity, this penalizes optical transparency. The relationship between the electrical conductivity ( $\sigma_c$ ) and the doping concentration ( $n$ ), and minority carrier lifetime ( $\tau$ ), is expressed in Eq. 6.

$$\sigma_c = ne^2 \frac{\tau}{m^*} \quad (6)$$

where  $e$  is the unit electronic charge, and  $m^*$  is the effective mass of the electron.  $n$  and  $\tau$  cannot be independently increased for TCOs having high carrier concentrations; charge transport is limited mainly by ionized impurity scattering, and optical transmission decreases at the near-infrared edge when doping concentration increases. Meanwhile, low  $m^*$  and high-quality materials with minimal defect content (allowing greater  $\tau$ ) are key features of TCOs possessing high electrical conductivity. Therefore, TCO layers having high carrier mobilities allow superior lateral conductivity that is essential to overcome the front surface optical transparency and electrical performance trade-off in SHJ solar cells. For even higher optical transparency up to 99.9% and lower sheet resistance below 5 Ω/sq., high-performing TCOs have been introduced recently through optimizations of the physical properties such as structural geometries and mass densities [93,94]. Numerical analysis revealed that TCOs having WF > 5 eV are preferable for state-of-the-art SHJ device design, i.e., allowing for thinner and lightly doped a-Si:H films [95]. Thus, advanced contact-related designs could reduce the opto-electrical losses through high-performance field-effect passivation and carrier-selectivity [93,94].

Besides having the most favorable electrical and optical properties, high thermal resilience and a low temperature coefficient are important features for photovoltaic front contact schemes. To appreciate the importance of accounting for thermal effects, we refer to the simple built-in junction potential model (Eq. 7) in semiconductor engineering for an idealized, abrupt p-n junction. The  $J_{sc}$  of the SHJ solar cell depends on the extent of the built-in voltage  $V_{bi}$  between the a-Si:H(i) layer and c-Si as a mechanism for charge separation and extraction, but which may be impeded by a high sheet resistance of the TCO. The maximum voltage that the solar cell can provide ( $V_{bi} = V_{oc}$ ) is subjected to the generation rate of excess electrons ( $\Delta n$ ) or holes ( $\Delta p$ ) in the active regions in which front contact optical transparency is vital [96]:

$$V_{oc} \equiv \frac{E_{FN} - E_{FP}}{e} = \frac{k_B T}{e} \ln \left( \frac{(n_0 + \Delta n)(p_0 + \Delta p)}{n_0 p_0} \right) \quad (7)$$

where  $n_0$  or  $p_0$  is the equilibrium electron or hole concentration, respectively, and the excess carrier density implies  $V_{oc}$  commensurate with the separation of the quasi-Fermi levels  $E_{FN}$  and  $E_{FP}$  at the n and p regions, respectively. As much as the  $\frac{n p}{n_0 p_0}$  ratio increases through carrier injection effects,  $V_{oc}$  is greater for a given temperature. Therefore, the temperature-sensitive  $J_{sc}$  characteristics implied by the irradiance depend on the properties of the active layer material. For optoelectronics, optical and electrical loss reduction approaches have been reported in several cases of not just adopting TCOs, but metal nanowires [94,97,98] and 2D materials [93,99,100,101]. This is in addition to front metal contact layers that comprise doped and dopant-free contacting schemes [102].

The pronounced trade-off relationship between optical transparency (or optical absorption/reflection) and electrical conductivity (or  $R_s$ ) is addressed in the literature for advanced contact schemes on the SHJ solar cell [96,102]. Several ideas, such as replacing the doped a-Si:H layer by a wider bandgap a-SiO<sub>x</sub>:H [103–106] or a-SiC<sub>x</sub>:H [107,108] layer, increasing the index contrast by inserting a dielectric layer such as MgF<sub>2</sub> between the TCO layer and metal grid [109], adopting conformal ALD-TCOs [110], or an enhanced MIS contact [111], etc., to alleviate the

$V_{oc}$  and FF trade-off, were also highlighted. A major contributor to the low FF is also believed to be due to the WF mismatch between the various contact layers, e.g., forming a Schottky barrier between the TCO and a-Si:H(p) layers thereby raising  $\rho_c$  and in turn impeding effective charge transport. Hence, besides optimizing the doping concentration, other approaches that have been explored to tune its WF include optimizing the deposition [112], plasma treatment [113], or chemical treatment [114], of the TCO layer. Alternatively, the WF of the doped a-Si:H layer may be tailored by increasing its doping concentration or otherwise be replaced by a doped poly-Si:H layer [115]. A high-WF buffer layer, such as In<sub>2</sub>O<sub>3</sub> [116] or MoO<sub>x</sub> [117] may also be inserted between the TCO and doped a-Si:H layers. Fig. 5 shows a TCO-/MoO<sub>x</sub>/a-Si:H(p)/a-Si:H(i) stack proposed for the back contact [117], which realized overall efficiency enhancements compared to that of a-Si:H(i)/a-Si:H(p)/TCO through favorable adjustment of the barrier height at the interface between the TCO and doped a-Si:H layers to reduce  $\rho_c$  and increase  $V_{oc}$  and FF. Besides SiO<sub>x</sub> or AlO<sub>x</sub>, the TCO contact structure may also typically employ TMOs such as sub-stoichiometric TiO<sub>x</sub> or MoO<sub>x</sub>, having a band gap > 3 eV and WF > 5 eV, to replace the a-Si:H(p) layer. MoO<sub>x</sub> (x < 3) exhibited best-in-class results with the selective hole contact scheme for n-Si solar cell FF and efficiency due to advantages in processing and optical transparency [75,118,119]. Sputter deposition of the TCO film atop the transparent MoO<sub>x</sub>-based HCL stack to form the efficient hole-selective front side contact grants effective carrier selectivity, and reduced parasitic absorption and  $\rho_c$ , hence attaining more than 19%-efficiency [76]. State-of-the-art designs can be guided by the fact that contact losses can be minimized dramatically utilizing the low-WF TiO<sub>x</sub> as the ECL and high-WF MoO<sub>x</sub> for hole-selective purposes [27,57,75,77,118,119].

### 2.3. On other CSC design concepts

Commonplace in industry is the textured front surface of a boron-diffused p<sup>+</sup> emitter passivated using an Al<sub>2</sub>O<sub>3</sub>/SiN<sub>x</sub> stack [26,41,80]. The industrially viable transparent TiO<sub>x</sub> layer thickness in the contact layer determines the  $V_{oc}$  and FF through the trade-off between surface passivation and  $\rho_c$ . The now-familiar thin SiO<sub>x</sub> layer in TOPCon technology was recently introduced, along with extremely-low-WF alkaline metals (in place of an n<sup>+</sup>-poly-Si layer), such as Mg, to create effective electron-selective contacts on n-type IBC solar cells [120]. Due to band alignment with the low-WF metal, the SiO<sub>x</sub> provides superior electron selectivity, and the use of a thin dielectric tunneling barrier at the metal-semiconductor interface has been experimentally demonstrated to reduce the  $\varphi_B$  effect at the interface, and hence the contact resistance. However, besides alleviating FLP, the implementation of a tunnel barrier introduces a tunneling resistance at the contact. It is imperative to understand the trade-off between the additional tunneling resistance and the reduced Schottky barrier resistance. In this way,  $\rho_c$  reduction can be optimized, in turn achieving a high FF and efficiency. It is noteworthy that while a thinner TCD layer permits quantum mechanical tunneling, and hence reduces  $\rho_c$ , atomic passivation may suffer, thereby increasing  $J_0$ . Annealing the contact layers dramatically reduces  $\rho_c$  and increases FF, whereas increasing the passivation layer thickness decreases surface/interface recombination at the penalty of a high  $\rho_c$  [121]. Despite a high interface state density (D<sub>it</sub>), the bilayer SiO<sub>x</sub>/Mg passivation film also enables outstanding electron selectivity thus yielding superior quantum efficiency and  $iV_{oc}$ . Moreover, with a TMO having a high WF and excellent optical transparency such as MoO<sub>x</sub>, superior hole-selectivity in tandem with a-Si:H(i) passivation of the front surface is predicted to achieve a 21.8%-efficiency [120]. Further, the MoO<sub>x</sub> layer thickness dictates the lateral conductivity to the contacts.

Effective field-effect and chemical passivation schemes have been demonstrated using PECVD-grown AlO<sub>x</sub>/SiN<sub>x</sub> dielectric stacks to passivate heavily doped p-Si emitters [122,123], thus enabling a simple cell structure fully compatible with existing industry production lines and processes for low-cost n-type bifacial solar cells. TiO<sub>x</sub>/SiO<sub>x</sub>

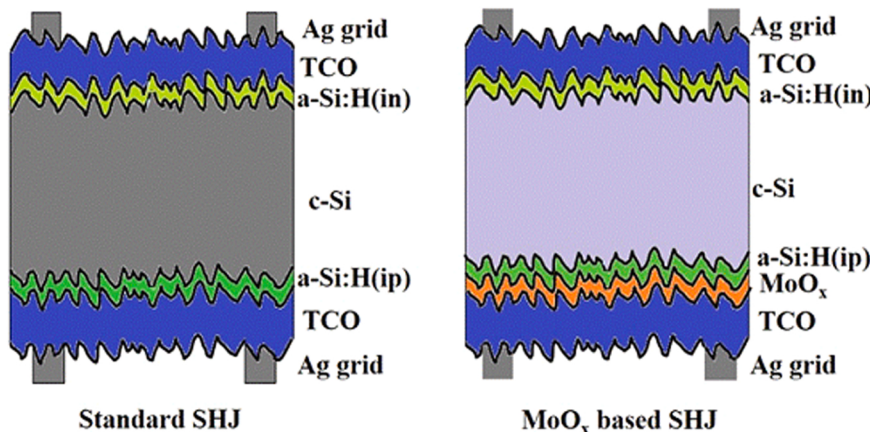


**Fig. 5.** Structure schematic illustrating the standard SHJ and modified SHJ incorporating an ultrathin MoO<sub>x</sub> buffer IL in the TCO-based back contact passivating stack.  
(used with permission from [117]).

dielectric stacks also afford excellent passivation and simultaneous electron-selective properties on the n-type SHJ solar cell [124,125]. Finally, electron-selective, passivating contacts based on SiO<sub>x</sub>/n-poly-Si have also been reported [10,11,96], which are able to overcome high D<sub>it</sub> and dopant diffusion issues, etc. Charge transfer from monocrystalline-Si to poly-Si through the ultrathin SiO<sub>x</sub> layer is possible while the doping present in the poly-Si increases the conductivity, thereby representing a major pathway for the back contact design of n-type SHJ solar cells. Nevertheless, it is well-known that parasitic optical absorption in the UV/visible range on the front surface is significant due to a narrow bandgap  $\sim$  1.6–1.8 eV and high defect density, and the lateral resistivity is high when using doped a-Si:H as the passivating layer. Therefore, as hole-selective (electron-selective) contacts, MoO<sub>x</sub> (bilayer SiO<sub>x</sub>/TiO<sub>x</sub> or SiO<sub>x</sub>/poly-Si) films have been considered to be industrially and technologically superior alternatives compared to doped a-Si:H. For a given dielectric stack passivation, charge transport and optical efficiency are reliant on important parameters such as the IL thickness, deposition technique adopted, and processing conditions.

### 3. Comparison between a-Si:H(p) and MoO<sub>x</sub> layers for front surface contacts

The fact that a doped a-Si:H layer allows excellent carrier selectivity is renowned, as well as its ability to act as a passivating layer. However, major shortcomings include the toxicity of material sources associated with doping, as well as the technological impact of front surface parasitic absorption. On the other hand, the tremendous potential in introducing an ultrathin MoO<sub>x</sub> film to act as a passivating and carrier-selective contact material is derived from its high WF compared to that of several other TMOs. Moreover, having among the lowest melting points compared to other TMOs, it is compatible with low-temperature deposition processes. Passivating contacts using MoO<sub>x</sub> have been realized on both n- and p-Si absorbers [37,75,118,119,126], and the success of MoO<sub>x</sub>-based passivating HCL stacks in SHJ solar cells has been widely reported [27,30,37,40,43,44,75,77,117–120,126,127]. Directly depositing MoO<sub>x</sub> on the p-Si absorber to form the back surface ohmic contact, and atop the front surface a-Si:H(i) passivating film on the n-Si absorber, were shown to improve current density and efficiency [118,119]. Due to the wider bandgap ( $\sim$  3 eV), the greater optical transparency of the MoO<sub>x</sub> layer results in improved optical gain compared to that of a-Si:H (p) at the hole-selective contact, which in principle, increases J<sub>sc</sub>. The optoelectric properties of MoO<sub>x</sub> are variable due to oxygen-vacancy defects that may create n-type conductivity. Charge carrier recombination at the MoO<sub>x</sub>/c-Si interface can be suppressed via a chemically-grown SiO<sub>x</sub> buffer layer on the c-Si surface prior to the MoO<sub>x</sub>

film deposition. In MoO<sub>x</sub>-passivated CSCs, the energy barrier at the hole contact is crucial to minimize leakage currents, but compared to a-Si:H (n)-passivated CSCs, the contact resistance is higher, and FF is lower. Hence, IL passivation, deposition, and subsequent processing need to be optimized to fine-tune the energy barrier for improved contact performance benefits [119].

#### 3.1. MoO<sub>x</sub> passivation: stoichiometric effect

The band-to-band tunneling afforded by the ultrathin MoO<sub>x</sub> passivating layer can reduce ρ<sub>c</sub> that is in turn dependent on passivation and energy barrier effects. Assuming FLP effects are trivial, MoO<sub>x</sub> typically forms a hole inversion layer at the n-Si surface, or hole accumulation layer at the p-Si surface, thus reducing ρ<sub>c</sub> [128]. Representative current-voltage measurements exhibiting ohmic behavior and the corresponding ρ<sub>c</sub> values are extracted for three different contact structures as shown in Fig. 6, for an MoO<sub>x</sub> IL thickness of  $\sim$  10 nm.

As the capping layer on a-Si:H(i) for front surface passivation, Paduthol et al. [129] reported that the use of SiN<sub>x</sub> is preferred over doped a-Si:H because the latter was found to adversely affect the carrier injection efficiency. The a-Si:H(i)/SiN<sub>x</sub> layer stack provides excellent surface passivation on c-Si, but suffers from a very high contact resistance. Only a small proportion of charge carriers generated in the a-Si:H (i) layer by light absorption contribute to the photocurrent [130]. Earlier analyses [37,75,118–120,126,127] have shown that the incorporation of an a-Si:H(i)/MoO<sub>x</sub> passivating stack enhances charge transport in the SHJ solar cell. Nevertheless, the extent of reduction in J<sub>0</sub> and ρ<sub>c</sub> is a function of the stoichiometry of the MoO<sub>x</sub> film, which in turn depends on the deposition technique and processing conditions. Chemical vapor deposition (CVD) [131], ALD [64,73], electron-beam evaporation [132], sputtering [133], and thermal evaporation [134–139] are common deposition techniques. The quality of charge transport is subjected to the band alignment at the c-Si/a-Si:H(i)/MoO<sub>x</sub> interfaces, as well as the presence of oxygen vacancy defect states within the MoO<sub>x</sub> film. The deposition-dependent WF [140,141] and passivation, as well as the wafer type, are responsible for the marked variation in the photoelectric parameters [142]. Low-temperature deposition caters to better control of the oxygen stoichiometry to attain superior crystallinity and optical transparency [141,142]. The presence of defects and IL band mismatch, however, represents technological challenges in obtaining high stability and efficiency performance. Therefore, there has been a range of attempts to overcome these problems. Recently, Mallem et al. [143] thermally evaporated stoichiometric MoO<sub>x</sub> films of high broadband optical transmittance, allowing the demonstration of 20%-conversion efficiency. Decent intrinsic thermal stability was realized for

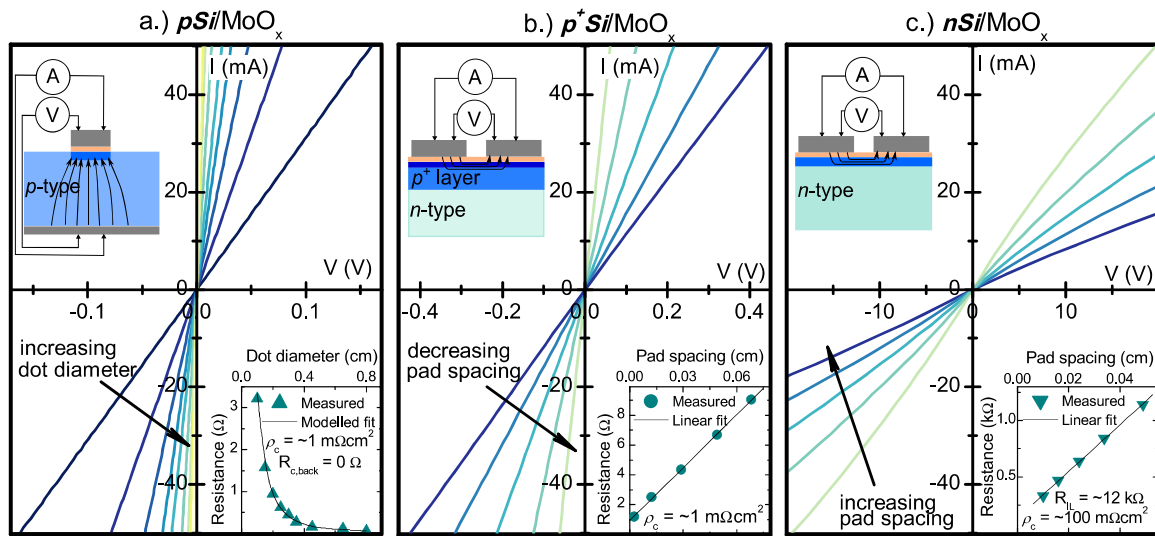


**Fig. 6.** Current-voltage measurements and  $\rho_c$  extraction for (a) p-Si/MoO<sub>x</sub>, (b) p<sup>+</sup>-Si/MoO<sub>x</sub>, and n-Si/MoO<sub>x</sub> contact structures with a fixed MoO<sub>x</sub> IL thickness of  $\sim 10 \text{ nm}$ .

(used with permission from [128]).

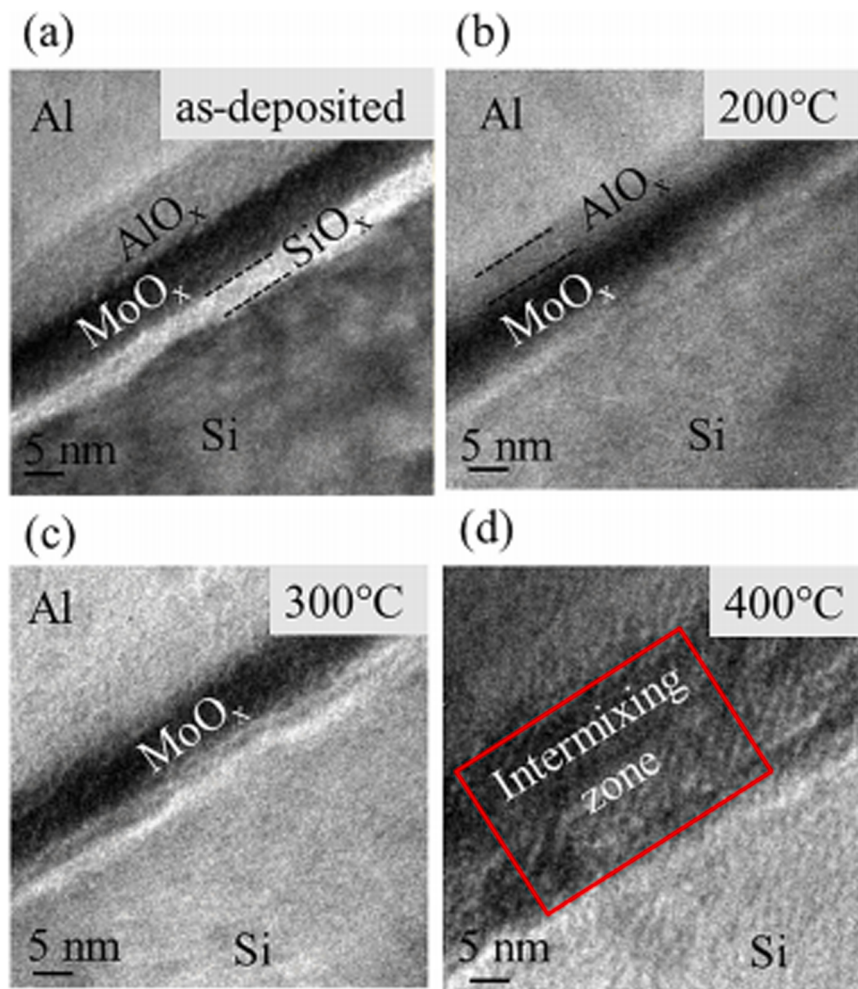


**Fig. 7.** Cross-sectional high-resolution TEM micrographs of the c-Si/MoO<sub>x</sub>/Al stack (a) as-deposited, and (b) annealed at 200 °C, (c) 300 °C or (d) 400 °C, for 10 min. (used with permission from [148]).

the annealed a-Si:H(i) layer prior to MoO<sub>x</sub> deposition, leading to a high current density and efficiency of 19.3% [144]. The annealing temperature, and thicknesses of the MoO<sub>x</sub> and a-Si:H(i) layers, are crucial for excellent charge transport properties and performance stability. Reduced  $\rho_c$  and improved optical transparency are obtained for a thinner MoO<sub>x</sub> layer so that the  $J_{sc}$  increases. However, while MoO<sub>x</sub> is an efficient hole collector, its optoelectronic properties may deteriorate during solar cell manufacture and processing. Before and after contact sinter annealing, oxidization reduces the MoO<sub>x</sub> WF and increases  $\rho_c$ , thereby degrading the photoelectrical performance. The annealing and plasma processing conditions, and the degree of stability of the deposited MoO<sub>x</sub> layer, may determine to what extent, if any, an interfacial a-SiO<sub>x</sub> layer precipitates in the a-Si:H(i)/MoO<sub>x</sub> stack. Furthermore, unless a pre-MoO<sub>x</sub>-deposition annealing step of the a-Si:H layer is adopted, degradation of the MoO<sub>x</sub> film can occur upon annealing for screen-printed metallization due to hydrogen effusion from the abutting a-Si:H(i) layer, which will adversely affect hole extraction and transport from the c-Si wafer [145].

### 3.2. Interfacial SiO<sub>x</sub> layer effects

An undesirable thin SiO<sub>x</sub> layer may arise at the c-Si/MoO<sub>x</sub> interface after subjecting the post-MoO<sub>x</sub>-film-deposited c-Si surface to TCO deposition-related plasma conditions with [143,144,146] or without a-Si:H(i) passivation [147,148]. Fig. 7 elucidates the formation of an amorphous O-rich silicon layer (~ 2–3 nm thick) at the interface of c-Si/MoO<sub>x</sub> studied using transmission electron microscopy, before and after annealing. That the silicon oxide precipitates at the interface with or without prior etching of the c-Si wafer [77] has not yet been fully understood. A high-quality MoO<sub>x</sub> layer possesses superior optical and electrical properties [143,144], but the onset of an SiO<sub>x</sub> IL is associated with dissociation of MoO<sub>x</sub>, thus giving rise to significant parasitic absorption [146] and an energy barrier that impedes hole transport to the contact [77,144,146]. Hence, the degradation of the MoO<sub>x</sub> film caused by a decrease in O content lowers its WF and leads to optical and resistance losses. Recently, oxygen diffusion was observed across the c-Si/MoO<sub>x</sub> or a-Si:H(i)/MoO<sub>x</sub> interface, eventually forming a sub-stoichiometric SiO<sub>x</sub> IL with or without an a-Si:H(i) passivation layer [147]. The chemical interactions between the MoO<sub>x</sub> and c-Si, as well as oxygen vacancy diffusion, are thus likely to lead to the growth of the interfacial SiO<sub>x</sub> layer. A thin SiO<sub>x</sub> IL may enhance charge carrier transport through quantum-mechanical tunneling [66,144,147], but a thicker IL may result in an energy barrier for hole diffusion to the contact [77,146]. Mallem et al. [149] recently reported on oxygen dilution during the MoO<sub>x</sub> thin film synthesis by thermal vacuum evaporation, which reduced the WF, and thus, the hole injection efficiency into the contact layer. In sum, oxygen vacancies will significantly modify the MoO<sub>x</sub> composition, thus affecting the optical absorption, WF, and electrical conductivity of the material.

### 4. New pathways for passivating contacts

While the a-Si:H(i)/MoO<sub>x</sub>/ITO contact structure has been considered to be promising, it is vital to consider both its mechanical and thermal stability. In this case, the contact performance deteriorates due to MoO<sub>x</sub> degradation in the a-Si:H(i)/MoO<sub>x</sub> stack capped by an ITO layer. On the other hand, heterostructure devices with a simplified process consisting of ITO directly deposited on the n-Si substrate by RF magnetron sputtering led to a naturally formed ultrathin indium doped a-SiO<sub>x</sub> (a-SiO<sub>x</sub>(In)) layer at the interface that provides effective field-effect passivation, allows excellent charge transport via quantum tunneling and enables a high-performance hole-selective contact [150,151]. The WF offset between ITO (5.06 eV) and n-Si (4.35 eV) results in a built-in field that facilitates hole-selectivity, whereas the negative charge centers embedded in the a-SiO<sub>x</sub>(In) IL due to In ions and oxygen vacancies induce highly asymmetric conductivity that favors holes and reduces

recombination losses due to defects at the c-Si surface. In fact, defect-assisted quantum tunneling of the holes may occur due to the fixed charges in the a-SiO<sub>x</sub>(In) IL [151]. The excellent charge transport property provided by the resulting a-SiO<sub>x</sub>(In)/TCO stack, therefore, leads to a significantly reduced  $\rho_c$ , thereby increasing both FF and efficiency even without a MoO<sub>x</sub> IL.

However, the temperature-sensitivity to degradation of both ITO and MoO<sub>x</sub>, as well as the huge cost burden of the ITO processing, propel device technologists to strive for alternative strategies towards less expensive development of the front surface contact of c-Si solar cells. The adoption of ITO as the TCO layer, and copious amounts of Ag paste in front-side metallization, drive up photovoltaic production expenses (due to In scarcity and costs) in CSC technologies that could offset the performance efficiency benefits. However, recent investigations reported that the Ag paste can be replaced by Cu plating and that ITO can be replaced by ZnO, which will significantly decrease photovoltaic module production costs [152].

#### 4.1. Cost-effective strategies

ITO-free photovoltaics technologies will potentially be an industrial success. Nicolai et al. [153] demonstrated a SiN<sub>x</sub> passivation layer in place of an ITO-based electrode stack for the n-Si solar cell with SiO<sub>x</sub>/n-poly-Si and SiO<sub>x</sub>/p-poly-Si as the top electron and bottom hole selective stack, respectively.  $J_{sc}$  and  $V_{oc}$  increase in the absence of an ITO layer, while FF is critically dependent on the doping density, and hence electrical conductivity, of the front n-poly-Si ECL. Morales-Vilches et al. [154] recently reported that in place of ITO on the front side surface, the AZO/SiO<sub>2</sub> bilayer yielded a  $J_{sc}$  improvement by 0.4 mA/cm<sup>2</sup> and a maximum efficiency of 23% for the n-type SHJ solar cell. The AZO was used as the front TCO layer, which was capped with an SiO<sub>2</sub> layer as the anti-reflection coating, so that these samples demonstrated enhanced stability under damp-heat test conditions.

Effective passivation was also demonstrated using spin-coated SiO<sub>x</sub> layers having thicknesses exceeding 100 nm ( $\tau_{eff} > 1$  ms) based on the low-temperature perhydropolysilazane (PHPS) precursor, and when capped with an AlO<sub>x</sub>:H or SiN<sub>x</sub>:H layer, further increases  $\tau_{eff}$  to levels above 2 ms [155]. Underpinning the high  $\tau_{eff}$  compared to that due to passivation by a single AlO<sub>x</sub> or SiN<sub>x</sub> layer ( $\tau_{eff} \sim 500 - 750$   $\mu$ s), the synergy of chemical and field-effect passivation was considered to have been achieved by the SiO<sub>x</sub> layer containing a high density of positive fixed charges and hydrogenation of the silicon surface by H diffusion from the AlO<sub>x</sub>:H or SiN<sub>x</sub>:H. Besides SiO<sub>2</sub>, typically used dielectrics such as ZnO, Si<sub>3</sub>N<sub>4</sub>, Al<sub>2</sub>O<sub>3</sub>, MgF, TiO<sub>2</sub>, HfO<sub>2</sub>, ZnS, SiON, CeO<sub>2</sub>, etc., were surveyed for their optoelectric properties when applied to c-Si [156–160]. Greater anti-reflection and passivation capabilities are possible along the interface with the n<sup>+</sup>/p<sup>+</sup>-type bulk Si, in which isoelectronic properties and optical gain are crucial requisites. Among these dielectrics, isoelectronic SiO<sub>x</sub> ILs are employed in n-Si TOPCon technologies [24,25,53,54], and when combined with a composite TiO<sub>2</sub>/SiO<sub>2</sub> bilayer stack [41,80] back surface passivation can be attained for electron-selective contacts in commercial c-Si solar cells. Nevertheless, thicker dielectric layers afford better chemical passivation whereas thinner layers allow more effective field-effect passivation and quantum-tunneling so that  $J_{sc}$  increases and  $\rho_c$  decreases.

As opposed to the typical ITO/Ag stack, the electron-selective thermally evaporated-LiF<sub>x</sub>/LPCVD-ZnO/Al stack combined with the hole-selective thermally evaporated-MoO<sub>x</sub> with dual surface passivation by a-Si:H(i) layers of the n-Si DASH solar cell, yielded a best-in-class efficiency of 21.4% [161]. In their study, Ali et al. [148] reported minimal  $\rho_c$  using MoO<sub>x</sub>/Al-based front metal grid contacts for ITO-free technologies. Excellent ohmic contacts were realized with great resilience to degradation effects after low-temperature annealing. Compared to ITO/MoO<sub>x</sub>/a-Si:H(i) contacts, the annealing temperature effects on MoO<sub>x</sub>/Al contacts were striking. Nonetheless, a potentially high degree of manufacturability of c-Si solar cells has recently been illustrated using

full-area hole-selective ALD- $\text{VO}_x$  contacts (minimum  $\rho_c \sim 95 \text{ m}\Omega \text{ cm}^2$ ) allowing an average PCE of 21.4% or a maximum of 21.6%, and with a demonstrated high environmental stability (0.1-% point PCE reduction in 3 months) [69]. The touted promise of adopting ALD- $\text{VO}_x$  as the HCL followed directly from the aforementioned results, and the observation by Yang et al. [69] that the WF of the ALD- $\text{MoO}_x$  film in ref. [73] is likely too low to be highly efficient in a CSC, and that the analysis showed that the former offers superior surface passivation (at best  $J_0 \sim 40 \text{ fA/cm}^2$ ) on *c*-Si. Moreover, amongst the metal (oxy)nitrides investigated so far for full-area ECLs, only ALD-TaN<sub>x</sub> and ALD-TiO<sub>x</sub>N<sub>y</sub> have been known to enable efficiency values > 20% on n-Si solar cells. While surface passivation of *c*-Si by the TaN<sub>x</sub> layer is so far inferior to that obtainable by TiO<sub>2</sub> and TaO<sub>x</sub> films [80,87], a PCE value up to 20.1% was demonstrated [32]. On the other hand, the incipient success of deploying

TiO<sub>x</sub>N<sub>y</sub> is more promising. Unlike the adoption of solution-processed-/ALD-TiO<sub>2</sub>(ZnO) for the ECL which usually requires thermal annealing or elemental doping to attain a low  $\rho_c$  value, full-area ALD-TiO<sub>x</sub>N<sub>y</sub> contacts can exploit a best PCE of 22.3% without thermal annealing [34]. The experimental PCE value afforded by ALD-TiO<sub>x</sub>N<sub>y</sub> steadily surpasses the record efficiency for TiO<sub>2</sub> (22.1%) in a full-area contact structure on the *c*-Si wafer, which can be explained by the fact that the electrical conductivity and electron density in the TiO<sub>x</sub>N<sub>y</sub> are far higher than that in TiO<sub>2</sub>, which in principle, bestow superior  $\rho_c$  and electron selectivity, respectively.

Finally, a study based on life cycle costing and cost-breakdown analysis of representative SHJ designs revealed that prospective improvements in cell processing and module design could result in a sturdy decline in production costs, by reducing and substituting Ag

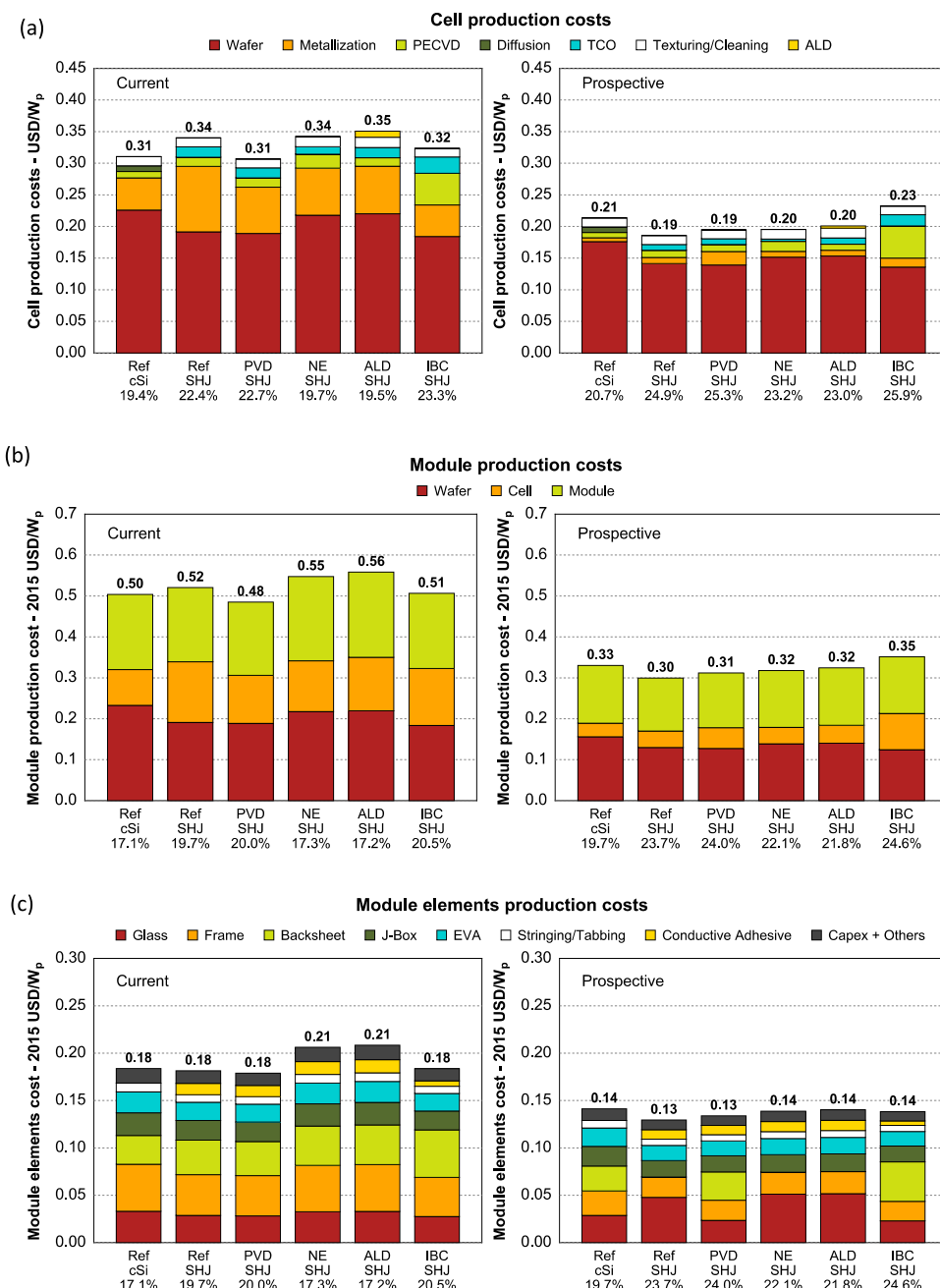


**Fig. 8.** Current and prospective (a) cell production costs, and (b) module production costs, for 5 SHJ designs and a baseline conventional monocrystalline silicon device; the percentages below the labels indicate the (a) cell and (b) module efficiencies. (c) Breakdown of the cost of module elements. (Used with permission from [152]).

consumption, increased cell efficiency and thinner wafers [152]. Fig. 8 shows the cell production costs (in USD/W<sub>p</sub>), the costs of complete photovoltaic modules, as well as the cost of the module materials, of selected technologies.

#### 4.2. Electrode fabrication: Industrial approach

Other than targeting low-cost processing, DASH solar cell efficiency upgrades have been due to passivation efforts to reduce recombination losses in the bulk as well as at the front and rear surfaces. To mitigate bulk recombination and contact losses, the use of thin wafer designs and advanced passivating IL schemes with high performance stability and production scalability have emerged. Thicker ITO layer coatings may reduce electrical resistivity losses, but other issues could arise such as increasing optical losses and production costs. A progressive approach to circumvent these issues involves PECVD-ILs to reduce processing costs. The various industry-standard passivation schemes adopted, and the corresponding techno-economic prospects are summed in Table 2.

Ag-printed SHJ solar cells having a thin front-side transparent electrode have already shown long-term performance reliability when capped with a PECVD-SiO<sub>x</sub> layer [162]. The 70-nm-thick PECVD-SiO<sub>x</sub> layer may act not only just as an anti-reflection layer, but as a barrier layer to protect the TCO from impurity diffusion due to the Cu plating. Nevertheless, mainstream industry production is evolving to higher efficiency PERC cell technology, and additional cost reductions, as well as further efficiency advancements, are expected from bifacial cell designs, and tandem stacked cell architectures [170]. The SiO<sub>2</sub>/SiN<sub>x</sub>:H passivation stack for c-Si solar cell front contacts significantly reduces the surface recombination current compared to that from conventional Al-BSF technology. With the same passivation stack on the rear surface, 21.3%-efficiency-SiO<sub>2</sub>-PERC cell technology can be realized [163]. The current standards of industrial PERC mass production can be upgraded by TOPCon technology on the high-efficiency, busbarless p-type bifacial cell, featuring a phosphorus diffused front emitter and p-poly-Si/SiO<sub>x</sub> passivated-rear surface [22].

Bulk (p-type c-Si) and surface (doped front emitter) recombination losses are key constraints, however, to the efficiency performance. New initiatives to reduce the parasitic absorption losses in the poly-Si were recently reported through various parameter investigations in the deposition and processing of the SiO<sub>x</sub>/n<sup>+</sup>-poly-Si passivating contact [171]. Poly-Si layer etching, as well as enacting the appropriate doping profile or doping technology, and optimizing the annealing conditions, are very effective to increase J<sub>sc</sub>, FF, and V<sub>oc</sub> of the SiO<sub>x</sub>/poly-Si rear-surface passivated contact cell. The ultrathin SiO<sub>x</sub> layer can be formed by various means, e.g., through thermal-, UV-ozone-, or wet-chemical-oxidation of the c-Si surface [172,173]. A detailed survey of the various approaches to growth or deposition of the ultrathin SiO<sub>x</sub> layer for emitter surface passivation [174] reported that while thermal SiO<sub>x</sub> featured the best passivation, its applicability in high volume manufacturing is limited because of its high thermal budget requisite. A low-temperature (~40 °C) chemical oxide passivation process based on using sodium hypochlorite solution (NCPRE-oxide) was proposed as feasible for industrial-scale implementation due to its low cost, low thermal budget, convenient waste disposal, and single component, safe chemical (unlike acids) solution preparation [175].

Surface treatment of the n<sup>+</sup>-poly-Si/SiO<sub>x</sub> passivating contacts, such as with forming gas annealing (FGA), ALD-AlO<sub>x</sub>:H, and PECVD-SiN<sub>x</sub>:H, increased τ<sub>eff</sub> and iV<sub>oc</sub>, through H-termination defect passivation at the c-Si/SiO<sub>x</sub> and SiO<sub>x</sub>/poly-Si interfaces (Table 2) [164]. Highly effective passivation was demonstrated when industry-relevant ultrathin (< 1.5 nm) tunnel SiO<sub>x</sub> layers were capped with heavily doped poly-Si, followed by subsequent passivation by an SiN<sub>x</sub> layer [165]. J<sub>0</sub> reduced greatly, and iV<sub>oc</sub> increased dramatically. An asymmetric, front-side textured electron-extracting contact, and rear-side planar hole-extracting passivated contact, led to an iV<sub>oc</sub> of 713 mV. Gao et al. [166] reported on an industry-compatible TOPCon architecture for

**Table 2**

Passivation and/or contact design and their related achievements reported in the literature.

Passivation stack and/or contact design	Key features of technology	Ref.
Introducing front and/or rear TOPCon on p-PERC architecture; rear surface passivation by p-poly-Si/SiO <sub>x</sub> stack.	TOPCon upgrade on p-PERC yielded a reduced contact recombination rate but increased parasitic absorption in the poly-Si layers resulting in an overall efficiency gain < 1%.	[22]
MoO <sub>x</sub> /Al layer stack deposited as hole-selective rear contact for p-Si solar cell.	Ultra-thin sub-stoichiometric SiO <sub>x</sub> interlayer formed at the MoO <sub>x</sub> /c-Si interface allows conduction of charge carriers; MoO <sub>x</sub> /Al contact layer exhibits minimal ρ <sub>c</sub> as low as 32 mΩ·cm <sup>2</sup> and is stable upon annealing up to 200 °C.	[148]
ITO replaced by multifunctional ALD-Al <sub>2</sub> O <sub>3</sub> / sputter-deposited ZnO window layer on the front side and Cu-plated contacts (with IBC design).	Huge reduction in Ag metallization and indium use results in lower prospective cell and module production costs; > 23%-efficiency.	[152]
Emitter metal directly contacts the front-surface n-poly-Si capped with a SiN <sub>x</sub> passivation layer in place of the ITO/AZO-based electrode stack.	ITO-free solar cell featuring poly-Si on front and rear passivating contacts; 19.2% efficiency measured on the planar surface.	[153]
Front TCO (AZO) and a-SiO <sub>2</sub> anti-reflection bilayer stack on monofacial rear emitter n-type SHJ solar cell.	Full-sized 244 cm <sup>2</sup> cells with double antireflection layer configuration showed J <sub>sc</sub> improvement and enhanced stability under damp-heat test conditions; 23%-efficiency.	[154]
Surface passivation of an n-Si wafer by SiO <sub>x</sub> /SiN <sub>x</sub> or SiO <sub>x</sub> /AlO <sub>x</sub> stack. Cu plating metallization scheme using a PECVD-SiO <sub>x</sub> capping layer on the ITO transparent electrode, with a-Si:H passivation layers.	Effective minority carrier lifetime, τ <sub>eff</sub> > 2 ms is achieved. Lowered production costs, with record-breaking efficiency of 26.7% for the SHJ solar cell.	[155]
SiO <sub>2</sub> /SiN <sub>x</sub> :H as front passivation stack on p-type SHJ solar cell; SiO <sub>2</sub> /SiN <sub>x</sub> :H stack on the rear surface of PERC architecture.	Replacing the Al-BSF contact by a SiO <sub>2</sub> /SiN <sub>x</sub> :H stack has markedly reduced J <sub>0</sub> and increased the efficiency by 0.2–20.1%; with SiO <sub>2</sub> /SiN <sub>x</sub> :H stack on the rear surface, long wavelength response is increased, and the rear surface recombination is suppressed with a low surface recombination velocity of 26 cm/s post-annealing. The efficiency increased by 1.3–21.3% compared to conventional Al-BSF solar cells.	[163]
n-poly-Si/SiO <sub>x</sub> passivating contacts capped by ALD-AlO <sub>x</sub> :H or PECVD-SiN <sub>x</sub> :H	Post-deposition forming gas annealing (FGA) increased the minority carrier lifetime to 12.5 and 5.4 ms and implied V <sub>oc</sub> to 728 and 727 mV, respectively, for 100 and 2 Ω□cm n-type c-Si substrates.	[164]
Electron-selective thermal-SiO <sub>x</sub> /n <sup>+</sup> -poly-Si and hole-selective thermal-SiO <sub>x</sub> /p <sup>+</sup> -poly-Si passivated contacts	Efficiency ~ 24%; iV <sub>oc</sub> of 690/703 mV on planar/textured c-Si surface; further improvement in minority carrier lifetime and iV <sub>oc</sub> , and reduced J <sub>0</sub> when capped with an SiN <sub>x</sub> layer to reduce parasitic absorption.	[165]
n <sup>+</sup> -poly-Si contact layer with ultrathin SiO <sub>x</sub> passivation obtained from PECVD a-Si:H with in-situ doping and high-temperature annealing.	p-type c-Si solar cell with rear n <sup>+</sup> -poly-Si TOPCon emitter yielding ~22.8 to ~24.9% efficiency.	[166]
Bifacial industrial TOPCon on a large-area n-type c-Si substrate; thermal-SiO <sub>x</sub> capped by n <sup>+</sup> /p <sup>+</sup> -poly-Si with PECVD-SiN <sub>x</sub> :H layer on rear/front side; screen-printed front/rear metallization.	TOPCon cells fabricated with a lean process flow compatible with mass production in pre-existing Al-BSF c-Si production line; J <sub>0</sub> ~ 2.6 fA/cm <sup>2</sup> , V <sub>oc</sub> > 700 mV, and 23% efficiency.	[167]

(continued on next page)

**Table 2 (continued)**

Passivation stack and/or contact design	Key features of technology	Ref.
Boron diffused front emitter, rear-side tunnel-SiO <sub>x</sub> /n <sup>+</sup> -poly-Si/SiN <sub>x</sub> :H, front/rear screen printed Ag electrodes	J <sub>0</sub> ~ 1.3 and 3.7 fA/cm <sup>2</sup> on polished and textured c-Si surfaces, respectively. After printing the Ag contacts, J <sub>0</sub> increased to 50.7 fA/cm <sup>2</sup> on the textured c-Si surface; median efficiency of 23.91%.	[168]
TOPCon on n-type c-Si wafer featuring a boron-diffused emitter and SiN <sub>x</sub> /AlO <sub>x</sub> passivation stack on the front side, and a passivating rear contact consisting of a SiN <sub>x</sub> /n-poly-Si/SiO <sub>x</sub> stack; fully screen-printed metal contacts on front/rear side.	V <sub>oc</sub> ~ 689.4 mV, FF ~ 81.35%, efficiency ~ 22.43%.	[169]

high-efficiency solar cells. The symmetrically passivated bifacial sample was realized on a p-Si wafer using an n<sup>+</sup>-poly-Si/SiO<sub>x</sub> stack, fabricated from the PECVD-a-Si:H precursor under optimized annealing and doping conditions. High-quality passivation was achieved, and J<sub>0</sub> = 3 fA/cm<sup>2</sup>, ρ<sub>c</sub> = 2 – 4 mΩ cm<sup>2</sup> and iV<sub>oc</sub> = 742 mV, with a prospective efficiency > 22.8%, were projected for industrial production.

Chen et al. [167] introduced double-side screen printing metallization on a textured bifacial n-Si cell structure incorporating industrially-favored TOPCon technology. The front boron-doped emitter was passivated by a thin film stack, while the rear surface n<sup>+</sup>-poly-Si was passivated by a PECVD-SiN<sub>x</sub>:H layer. The passivation effect of the SiO<sub>x</sub>/n<sup>+</sup>-poly-Si stack resulted in a low J<sub>0</sub> of 2.6 fA/cm<sup>2</sup>, and V<sub>oc</sub> > 700 mV and 23%-efficiency were achieved. More recently, a median efficiency of 23.9% and minimal J<sub>0</sub> were reported for large-area n-type industrial TOPCon silicon solar cells (Fig. 9), based on a cell structure with a boron diffused front emitter, rear side tunnel-SiO<sub>x</sub>/n<sup>+</sup>-poly-Si/SiN<sub>x</sub>:H structure, and screen-printed electrodes on both sides [168]. Industrial TOPCon cells with efficiency, V<sub>oc</sub>, and FF, as high as 22.43%, 0.689 V, and 81.35%, respectively, were obtained [169]. In this case, the phosphorus dopant diffusion in the poly-Si layer, and the thickness of the SiO<sub>x</sub> layer, were optimized to obtain a suitably high-performing electrical contact between the screen-printed Ag and the c-Si. A SiO<sub>x</sub> layer thickness exceeding 1.5 nm was recommended for high-quality passivation. In lieu of the customary PERC cells, full-area Al-BSF with rear-side Al grid contact is promising in mainstream cell production. Furthermore, SHJ, TOPCon, cost-effective thin wafer c-Si technologies, as well as low-cost c-Si bifacial PERC solar cells, are within the framework of near-future industrial deployments [176,177].

#### 4.3. Passivation stacks: An industry-based analysis

At present, the use of SiO<sub>x</sub>-, SiN<sub>x</sub>- and AlO<sub>x</sub>-based TCD passivation stacks has much potential in industrially-compatible PERC, HIT, POLO

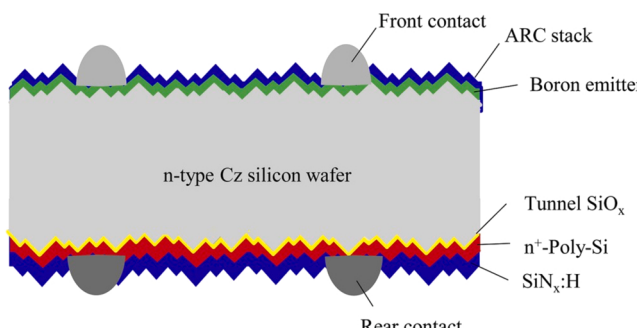


**Fig. 9.** Schematic illustrating an i-TOPCon solar cell on n-type c-Si wafer. (Used with permission from [168]).

or TOPCon technologies. The passivating materials contain different fixed charge polarities: AlO<sub>x</sub> possess negative fixed charges [2], [178] while SiO<sub>x</sub> [7], [155] and SiN<sub>x</sub> have positive fixed charges [8]. Other key attributes of passivation layers are a high reflective index, a wide bandgap, and high thermal resilience. Such surface and interface passivation layers may be deployed alongside stable poly-Si passivation layers that can withstand industrial firing thermal treatment processes. Thermal deposition, post-annealing, and high-temperature firing (e.g., in an infrared conveyor-belt furnace) are standard processes to maintain high optical transparency and excellent passivation properties in the c-Si solar cell industry. For example, as a single, rapid (< 10 s) post-deposition annealing (> 800 °C) step, partial crystallization can be attained of amorphous material to effectuate charge carrier accumulation in the near-surface region. Further, the replacement of costly high-temperature deposition processes by PECVD, ALD, and atmospheric pressure chemical vapor deposition (APCVD), is seen to be very important. Hence, low-cost, facile processes to develop TCDs with superior optoelectronic properties are highly sought after. It is understood that ALD-AlO<sub>x</sub> films and ALD-AlO<sub>x</sub>/SiO<sub>x</sub> stacks have shown high-quality passivation properties leading to reduced surface recombination velocities and high τ<sub>eff</sub> [179]. Compared with a single layer AlO<sub>x</sub> or SiO<sub>x</sub>, the AlO<sub>x</sub>/SiO<sub>x</sub> bilayer allowed superior chemical passivation due to the greater amount of H atoms that saturate the dangling bonds on the c-Si surface, thus decreasing D<sub>it</sub> [179]. However, although the total passivation increased, capping the AlO<sub>x</sub> layer with SiO<sub>x</sub> modified the fixed charge density Q<sub>f</sub> from  $-1.6 \times 10^{12}/\text{cm}^2$  to  $-1.3 \times 10^{12}/\text{cm}^2$ , thus indicating that any change in field-effect passivation was greatly offset by chemical passivation [179]. Earlier, Laades et al. [180] reported that when capping the PECVD-AlO<sub>x</sub>/SiN<sub>x</sub> stack with SiO<sub>x</sub>, not only can a high degree of chemical passivation be achieved through saturation of dangling bonds by H atoms, but post-deposition thermal treatment and firing can increase the negative fixed charge density. Thus, notable gains in τ<sub>eff</sub> and iV<sub>oc</sub> can be realized. Meanwhile, it should be considered that the passivation afforded by an AlO<sub>x</sub>/SiO<sub>x</sub> stack, which was performed on n-Si substrates in ref. [177], or on p-Si substrates in ref. [180], is not similar [153]. In the latter, the magnitude increase in -Q<sub>f</sub> can be associated with a spike in the density of negatively charged AlO<sub>4</sub> tetrahedra at the AlO<sub>x</sub>/SiO<sub>x</sub> interface after a thermal treatment step. The SiO<sub>x</sub> layer by itself may provide different passivation properties depending on whether they are grown by thermal or wet chemical processes. Typically, the SiO<sub>x</sub> layer endows limited chemical passivation but enacts effective field-effect passivation due to the inherent +Q<sub>f</sub>. Finally, the passivation properties may depend on the deposition- and processing-related fixed charge polarity, which differ at the c-Si/ SiO<sub>x</sub> and c-Si/AlO<sub>x</sub> interfaces. Thinner ALD-AlO<sub>x</sub> layers allow greater field-effect passivation than chemical passivation but capping with an SiO<sub>x</sub> layer (prepared by spin-coating using PHPS as the precursor and annealed at 450 °C) slightly reduces the field-effect passivation while greatly enhancing chemical passivation [179]. A similar trend was shown in ref. [41] for the TiO<sub>x</sub>/SiO<sub>2</sub> bilayer, where because of the reduced thickness of the TiO<sub>x</sub> film featured a reduced ρ<sub>c</sub> and field-effect passivation, but with the latter offset by an increased level of chemical passivation of the interface with the c-Si. Moreover, the passivation properties of the TiO<sub>x</sub>/SiO<sub>2</sub> stack do not degrade under concentrated sunlight [181].

Alternatively, doped poly-Si provides superior passivation quality for metal contacts compared to that found on mainstream diffused c-Si/ AlO<sub>x</sub> interfaces [182]. These poly-Si-based CSCs feature an interfacial oxide between the wafer and doped poly-Si, and are applied with industry-compatible processes on commercially available n-Si wafers, which for n-poly-Si obtained J<sub>0</sub> < 1 fA/cm<sup>2</sup> and iV<sub>oc</sub> of 741 mV, superior to that of p-poly-Si [183]. The results may be ascribed to the higher level of surface passivation quality enabled by n-poly-Si compared to that of p-poly-Si [184]. Hence, the n-poly-Si capped by a TCD layer/stack is industrially favorable since not only does this improve surface passivation, but also firing stability. Capping layers derived from H-rich TCDs

such as  $\text{AlO}_x$  [185,186] or  $\text{SiN}_x$  [187,188] serve as a source for hydrogenation of the  $c\text{-Si}/\text{SiO}_2$  interface [164,189,190], as well as to erect an effusion barrier to retain the hydrogen in the underlying film [191]. Mewe et al. [192] compared the passivating quality of the capping layer ( $\text{SiN}_x$ ,  $\text{Al}_2\text{O}_3$ ,  $\text{Al}_2\text{O}_3/\text{SiN}_x$ , or an  $\text{Al}_2\text{O}_3/\text{SiN}_x$ -based dielectric stack) on 200-nm-thick LPCVD-p-/n-poly-Si on textured surfaces of the IBC cell. It was observed that whereas the application of a single  $\text{SiN}_x$  layer with p-poly-Si resulted in interface passivation only after a firing step, the application of a single  $\text{Al}_2\text{O}_3$  layer initially provides a high level of passivation, but appears not to be firing stable with both p- and n-poly-Si because of the effusion of hydrogen. Hence, in order to enhance the firing stability, the  $\text{Al}_2\text{O}_3$  layer is usually capped with a PECVD- $\text{SiN}_x$  layer, which acts as an effusion barrier [193]. The n<sup>+</sup>/p<sup>+</sup>/i-poly-Si CSC passivated by a single layer, bilayer, or trilayer of  $\text{AlO}_x$ ,  $\text{AlO}_x/\text{SiN}_x$ , or  $\text{AlO}_x/\text{SiN}_x/\text{AlO}_x$  stack allow passivated emitter and rear polysilicon (PERPoly)/industrial TOPCon cell efficiency of up to 24% [183]. Record low contact recombination ( $J_0 \sim 65$  and 200 fA/cm<sup>2</sup> for n<sup>+</sup>- and p<sup>+</sup>-poly-Si, respectively) was achieved for screen-printed fire-through metal contacts [183]. The LPCVD- $\text{SiO}_x/\text{n}^+\text{-poly-Si}$  stack capped by PECVD- $\text{SiN}_x\text{:H}$  improved passivation through the healing of residual defects by hydrogen diffusion at the  $c\text{-Si}/\text{SiO}_x$  interface, thus resulting in  $iV_{oc}$  and implied fill factor (iFF) up to 735 mV and 87.5%, respectively [194]. For industrially relevant screen-printing, annealing of the uncoated n<sup>+</sup>-poly-Si decreased surface passivation likely due to contamination, but annealing of  $\text{SiN}_x\text{:H}$ -coated-n<sup>+</sup>-poly-Si did not improve passivation, as shown by the drastic reduction in  $iV_{oc}$  to 607 mV (from

720 mV) after 900 °C quick firing. Adding an interfacial  $\text{AlO}_x$  coating (which could act as an additional source of H atoms to saturate dangling bonds, and as a stabilizer to the effusion of H atoms from the n<sup>+</sup>-poly-Si structure) at the  $\text{SiN}_x\text{:H}/\text{n}^+\text{-poly-Si}$  interface, however, reduced the  $iV_{oc}$  only slightly, to 730 mV (from 735 mV) after the same firing step.

Improved passivation can also be achieved in the n-poly-Si-based CSC via application of H-rich TCOs [191]. Capping the rear-side  $\text{SiO}_x/\text{n}^+\text{-poly-Si}$  stack with an ALD-TCO (ITO or AZO) can endow excellent surface passivation and contact properties for both low- and high-temperature processes [194]. The  $\text{SiN}_x\text{:H}/\text{AlO}_x/\text{AZO}$  stack can preserve the high surface passivation properties of n<sup>+</sup>-poly-Si up to an 850 °C-firing-step [194]. Hence, overall passivation quality and optical and electrical gains can be significantly fortified by the multilayer stack passivation for IBC-SHJ and TOPCon technologies. In sum, while single-layer (such as poly-Si) passivation was shown to be highly susceptible to degradation under high-temperature industrial firing conditions, the solar cell performance parameters are more stable when using the appropriate passivating multilayered stack based on TCDs and/or TCOs. A thicker dielectric stack will reduce the effectiveness of field-effect passivation, as according to the simple model capacitor of Eq. 1, so that the predominant passivation mechanism in the total passivation is chemical passivation. It should be considered, however, that resistive losses may arise from newly-developed In-free TCOs following high-temperature processes, or from thin poly-Si layers that usually feature high sheet resistances [121,153,194]. Nevertheless, by fine-tuning the dielectric stack, the TCD sheet resistance can be reduced.

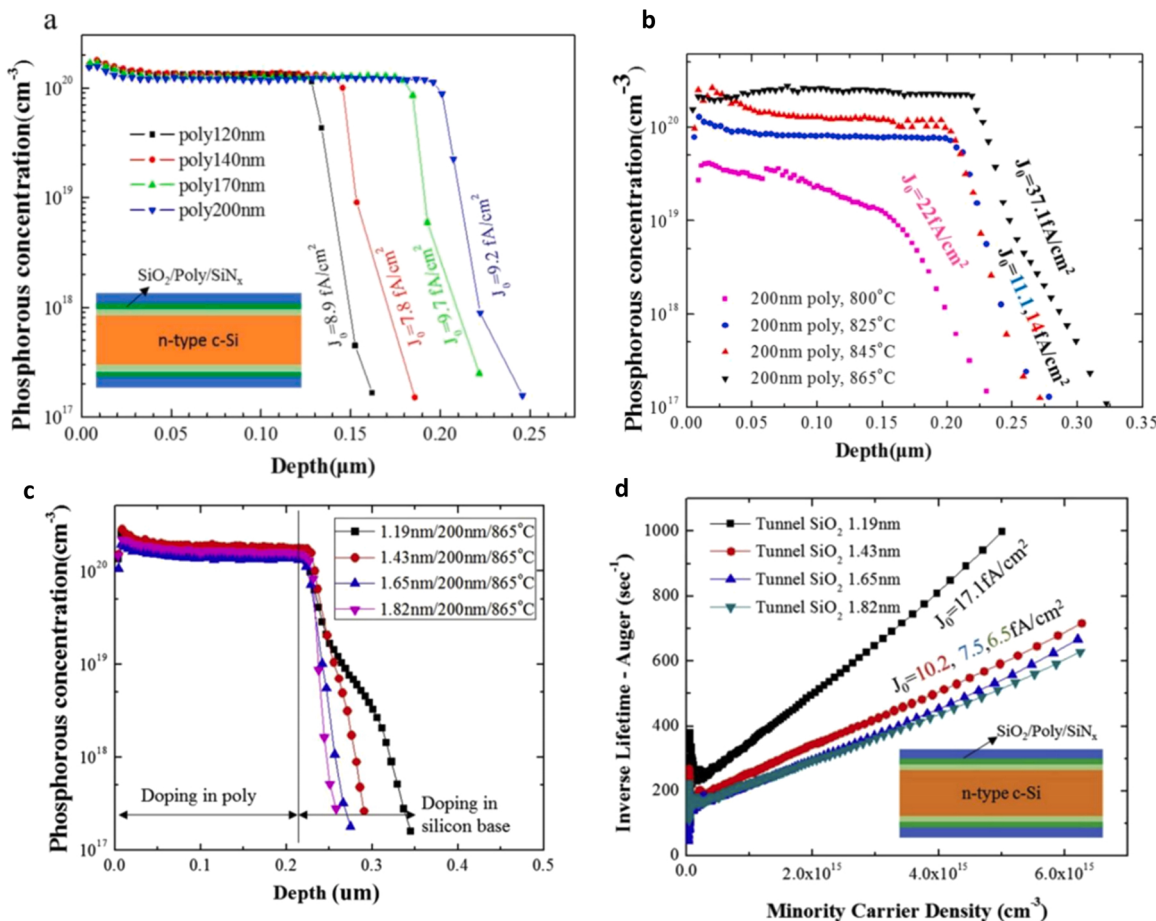


**Fig. 10.** ECV-measured phosphorus doping profiles below the surface, with various (a) poly-Si thicknesses ranging from 120 to 120 nm, (b) diffusion temperatures ranging from 800 °C to 865 °C, and (c) tunnel  $\text{SiO}_x$  thicknesses ranging from 1.19 to 1.82 nm. (d) The Auger-corrected inverse effective lifetime versus minority carrier concentration curves evaluated under high injection conditions. The corresponding  $J_0$  results, where present, are based on the symmetric  $\text{SiN}_x/\text{n}^+\text{-poly-Si}/\text{SiO}_2/\text{n}$ -type c-Si structure as shown in the inset of (a)/(d).

(Used with permission from [196].)

Moreover, ITO-free TCO alternatives such as doped AZO or FTO may slash device production costs. Further, bifacial n-Si PERT solar cells make use of a thin and uniform BSF layer achieved by phosphorus doping. So far, strategies to increase the performance-to-cost ratio have included optimization of the tunnel SiO<sub>2</sub> and poly-Si layer thicknesses, or of the phosphorus diffusion process (see Fig. 10) for the passivated contact structure to attain a high  $\tau_{\text{eff}}$  and to minimize free carrier absorption effects [195], [196]. In lieu of Ag paste printing and firing for metallization, Cu plating is being sought [150] for low production costs and high photovoltaic performance [162]. As an alternative to high-temperature processing, the use of appropriate multilayer passivating stacks has much potential in suppressing D<sub>it</sub> through H<sup>+</sup> diffusion and termination, and which can be optimized at low temperatures. Excellent cell performance parameters can be obtained by low-temperature PECVD and ALD fabrication of the passivated TCD, providing maximal cell efficiency at minimum production cost.

## 5. Concluding remarks

A wide range of CSC development pathways with lithographic back contacts has been reported to tackle the limited photovoltage and contact-related losses in mainstream solar cells. For doped a-Si:H-based CSCs, parasitic absorption, defect-assisted recombination, Auger recombination, and band gap narrowing losses, are the main loss mechanisms. Therefore, alternative dopant-free CSC designs have been addressed. Compared with mainstream c-Si technology, field-effect passivated IBC architectures, new IBC-SHJ and POLO junction or TOPCon structures, are realizing a lot of industrial potential. Charge carrier asymmetry due to accumulation or inversion at the surface induced by field-effect passivation through fixed charges in the thin dielectric passivating layer has been known to increase the carrier lifetime and charge transport, thereby leading to increased J<sub>sc</sub>, V<sub>oc</sub>, and efficiency – a valid premise for dopant-free CSCs. In DASH cells, MoO<sub>x</sub> and TiO<sub>x</sub> are popular material candidates for the HCL and ECL, respectively, which realize improvements to the photoelectric parameters through enhanced passivation and carrier-selective properties. Strong contenders arising for the HCL and ECL include VO<sub>x</sub> and TiO<sub>x</sub>N<sub>y</sub> films, respectively, due to their advantages in one or a combination of the following: surface passivation, carrier selectivity, electrical conductivity, and/or environmental-/photo-stability on c-Si. However, the industrial pre-requisite of performance resilience to thermal processing remains a key technical challenge.

The electro-optical performance when combining the transparent MoO<sub>x</sub> with SiO<sub>x</sub> and ITO layers as the hole-collecting stack has been addressed systematically. The use of PECVD- or ALD-SiN<sub>x</sub>, Al<sub>2</sub>O or the SiN<sub>x</sub>:H/AlO<sub>x</sub> bilayer passivation stack to cap n<sup>+</sup>-/p<sup>+</sup>-type poly-Si/SiO<sub>x</sub> in both IBC-SHJ and TOPCon cells have become remarkable choices for industry adoption. Manufacturing with low-cost industrial processes, combined with high throughput, high cell efficiency performance, and bifacial applications, are forthcoming considerations for the passivated contact stacks used in PERPolar bifacial solar cells or industrial TOPCon configurations.

## Declaration of Competing Interest

The authors declare that they have no known competing financial interests or personal relationships that could have appeared to influence the work reported in this paper.

## Acknowledgements

Dr. B.K.G. would like to thank University Malaysia Sabah (UMS) and he is greatly indebted to Prof. K.-W.A.C. of the University of Science and Technology of China (USTC) for accepting him into the opportunity to collaborate on this work. The crystalline silicon photovoltaic technology and cost roadmaps, Andrés Cuevas (Australian National University),

Stefaan De Wolf (King Abdullah University of Science and Technology), Christophe Ballif (Ecole Polytechnique Fédérale de Lausanne), Matin Hermle (Fraunhofer), Kenji Yamamoto (Kaneka Corporation), and Martin Green (University of New South Wales), are credited for instigating the writing of this review, and their invaluable reports have been key references. This work was supported by the Chinese Academy of Sciences (CAS). The award of various other funding sources is acknowledged by K.-W.A.C., such as the National Key Research and Development of China (2018 TFB1500103), Zhejiang Energy Group (znk-2018-118), the Ministry of Education of the P.R.C. (111 Project 2.0: BP0719016), BK21 project of the Ministry of Education of Korea, National Natural Science Foundation of China (61650110517) and Natural Science Foundation of Ningbo (2017A610095).

## Declarations

The authors have no conflicts to disclose.

## References

- [1] Z. Liu, et al., Revisiting thin silicon for photovoltaics: a technoeconomic perspective, *Energy Environ. Sci.* 13 (1) (2020) 12–23, <https://doi.org/10.1039/C9EE02452B>.
- [2] A. Blakers, Development of the PERC Solar Cell, *IEEE J. Photovolt.* 9 (3) (2019) 629–635, <https://doi.org/10.1109/JPHOTOV.2019.2899460>.
- [3] N. Balaji, et al., Pathways for efficiency improvements of industrial PERC silicon solar cells, *Sol. Energy* 214 (2021) 101–109, <https://doi.org/10.1016/j.solener.2020.11.025>.
- [4] F. Kløw, H. Haug, S.E. Foss, Surface recombination velocity measurements of metallized surfaces by photoluminescence imaging, *Energy Procedia* 43 (2013) 18–26, <https://doi.org/10.1016/j.egypro.2013.11.084>.
- [5] D. Ory, N. Paul, L. Lombez, Extended quantitative characterization of solar cell from calibrated voltage-dependent electroluminescence imaging, *J. Appl. Phys.* 129 (4) (2021) 43106, <https://doi.org/10.1063/5.0021095>.
- [6] B. Min, et al., A roadmap toward 24% efficient PERC solar cells in industrial mass production, *IEEE J. Photovolt.* 7 (6) (2017) 1541–1550, <https://doi.org/10.1109/JPHOTOV.2017.2749007>.
- [7] T. Dullweber, J. Schmidt, Industrial silicon solar cells applying the passivated emitter and rear cell (PERC) concept—a review, *IEEE J. Photovolt.* vol. 6 (5) (2016) 1366–1381, <https://doi.org/10.1109/JPHOTOV.2016.2571627>.
- [8] A. Cuevas, et al., Carrier population control and surface passivation in solar cells, *Sol. Energy Mater. Sol. Cells* 184 (2018) 38–47, <https://doi.org/10.1016/j.solmat.2018.04.026>.
- [9] N. Chatterji, A. Antony, P.R. Nair, Temperature coefficient of silicon-based carrier selective solar cells, *IEEE J. Photovolt.* 9 (3) (2019) 583–590, <https://doi.org/10.1109/JPHOTOV.2019.2892127>.
- [10] J. Melskens, B.W. Loo, B. Macco, L.E. Black, S. Smit, W.M.M. Kessels, Passivating contacts for crystalline silicon solar cells: from concepts and materials to prospects, *IEEE J. Photovolt.* 8 (2) (2018) 373–388, <https://doi.org/10.1109/JPHOTOV.2018.2797106>.
- [11] T.G. Allen, J. Bullock, X. Yang, A. Javey, S.D. Wolf, Passivating contacts for crystalline silicon solar cells, *Nat. Energy* 4 (2019) 914–928, <https://doi.org/10.1038/s41560-019-0463-6>.
- [12] K. Yoshikawa, et al., Silicon heterojunction solar cell with interdigitated back contacts for a photoconversion efficiency over 26%, *Nat. Energy* 2 (5) (2017) 17032, <https://doi.org/10.1038/nenergy.2017.32>.
- [13] D.E. Carlson, The status of amorphous silicon solar cells, *Photovolt. Sol. Energy Conf.* (1981) 294–301, [https://doi.org/10.1007/978-94-009-8423-3\\_42](https://doi.org/10.1007/978-94-009-8423-3_42).
- [14] M. Tanaka, et al., Development of new a-Si/c-Si heterojunction solar cells: {ACJ}-{{HIT}} (artificially constructed junction-heterojunction with intrinsic thin-layer), *Jpn. J. Appl. Phys.* 31 (1) (1992) 3518–3522, <https://doi.org/10.1143/jjap.31.3518>.
- [15] M.A. Green, et al., Solar cell efficiency tables (version 49), *Prog. Photovolt. Res. Appl.* 25 (1) (2017) 3–13, <https://doi.org/10.1002/pip.2855>.
- [16] S. De Wolf, A. Descoeuilles, Z.C. Holman, C. Ballif, High-efficiency silicon heterojunction solar cells: a review, *Green* 2 (1) (2012) 7–24, <https://doi.org/10.1515/green-2011-0018>.
- [17] A. Descoeuilles, Z.C. Holman, L. Barraud, S. Morel, S. De Wolf, C. Ballif, >21% efficient silicon heterojunction solar cells on n- and p-type wafers compared, *IEEE J. Photovolt.* 3 (1) (2013) 83–89, <https://doi.org/10.1109/JPHOTOV.2012.2209407>.
- [18] M. Taguchi, et al., 24.7% record efficiency HIT solar cell on thin silicon wafer, *IEEE J. Photovolt.* 4 (1) (2013) 96–99, <https://doi.org/10.1109/JPHOTOV.2013.2282737>.
- [19] D. Adachi, J.L. Hernández, K. Yamamoto, Impact of carrier recombination on fill factor for large area heterojunction crystalline silicon solar cell with 25.1% efficiency, *Appl. Phys. Lett.* 107 (23) (2015), 233506, <https://doi.org/10.1063/1.4937224>.

- [20] J. Haschke, et al., The impact of silicon solar cell architecture and cell interconnection on energy yield in hot & sunny climates, *Energy Environ. Sci.* 10 (5) (2017) 1196–1206, <https://doi.org/10.1039/C7EE00286F>.
- [21] A. Ingenito, et al., A passivating contact for silicon solar cells formed during a single firing thermal annealing, *Nat. Energy* 3 (9) (2018) 800–808, <https://doi.org/10.1038/s41560-018-0239-4>.
- [22] C. Messmer, A. Fell, F. Feldmann, N. Wöhrle, J. Schön, M. Hermle, Efficiency roadmap for evolutionary upgrades of perc solar cells by topcon: impact of parasitic absorption, *IEEE J. Photovolt.* 10 (2) (2019) 335–342, <https://doi.org/10.1109/JPHOTOV.2019.2957642>.
- [23] S. Choi, et al., Structural evolution of tunneling oxide passivating contact upon thermal annealing, *Sci. Rep.* 7 (1) (2017) 12853, <https://doi.org/10.1038/s41598-017-13180-y>.
- [24] D. Yan, A. Cuevas, S.P. Phang, Y. Wan, D. Macdonald, 23% efficient p-type crystalline silicon solar cells with hole-selective passivating contacts based on physical vapor deposition of doped silicon films, *Appl. Phys. Lett.* 113 (6) (2018), 61603, <https://doi.org/10.1063/1.5037610>.
- [25] S.W. Glunz et al., “The irresistible charm of a simple current flow pattern – approaching 25% with a solar cell featuring a full-area back contact,” in Proceedings of the 31st European Photovoltaic Solar Energy Conference and Exhibition, Hamburg, Germany, 2015, pp. 259–263. doi:10.4229/EUPVSEC20152015-2BP.1.1.
- [26] X. Yang, P. Zheng, Q. Bi, K. Weber, Silicon heterojunction solar cells with electron selective TiO<sub>x</sub> contact, *Sol. Energy Mater. Sol. Cells* 150 (2016) 32–38, <https://doi.org/10.1016/j.solmat.2016.01.020>.
- [27] J. Bullock, et al., Stable dopant-free asymmetric heterocontact silicon solar cells with efficiencies above 20%, *ACS Energy Lett.* 3 (3) (2018) 508–513, <https://doi.org/10.1021/acsenrgylett.7b01279>.
- [28] J. Ding, Y. Zhou, G. Dong, M. Liu, D. Yu, F. Liu, Solution-processed ZnO as the efficient passivation and electron selective layer of silicon solar cells, *Prog. Photovolt. Res. Appl.* 26 (12) (2018) 974–980, <https://doi.org/10.1002/pip.3044>.
- [29] J. Bullock, et al., Lithium fluoride based electron contacts for high efficiency n-type crystalline silicon solar cells, *Energy Mater.* 6 (14) (2016), 1600241, <https://doi.org/10.1002/aenm.201600241>.
- [30] W. Wu, et al., 22% efficient dopant-free interdigitated back contact silicon solar cells, *AIP Conf. Proc.* 1999 (1) (2018) 1–6, <https://doi.org/10.1063/1.5049288>.
- [31] Y. Wan, et al., Temperature and humidity stable alkali/alkaline-earth metal carbonates as electron heterocontacts for silicon photovoltaics, *Adv. Energy Mater.* 8 (22) (2018), 1800743, <https://doi.org/10.1002/aenm.201800743>.
- [32] X. Yang, et al., Tantalum nitride electron-selective contact for crystalline silicon solar cells, *Adv. Energy Mater.* 8 (20) (2018), 1800608, <https://doi.org/10.1002/aenm.201800608>.
- [33] J. Yu, et al., Titanium nitride electron-conductive contact for silicon solar cells by radio frequency sputtering from a TiN target, *ACS Appl. Mater. Interfaces* 12 (23) (2020) 26177–26183, <https://doi.org/10.1021/acsami.0c04439>.
- [34] X. Yang, et al., A highly conductive titanium oxynitride electron-selective contact for efficient photovoltaic devices, *Adv. Mater.* 32 (32) (2020) 1–8, <https://doi.org/10.1002/adma.202002608>.
- [35] E. Zojer, T.C. Taucher, O.T. Hofmann, The impact of dipolar layers on the electronic properties of organic/inorganic hybrid interfaces, *Adv. Mater. Interfaces* 6 (14) (2019), 1900581, <https://doi.org/10.1002/admi.201900581>.
- [36] C. Reichel, et al., Electron-selective contacts via ultra-thin organic interface dipoles for silicon organic heterojunction solar cells, *J. Appl. Phys.* 123 (2) (2018) 24505, <https://doi.org/10.1063/1.5010937>.
- [37] J. Bullock, C. Samundsett, A. Cuevas, D. Yan, Y. Wan, T. Allen, Proof-of-concept p-type silicon solar cells with molybdenum oxide local rear contacts, *IEEE J. Photovolt.* 5 (6) (2015) 1591–1594, <https://doi.org/10.1109/JPHOTOV.2015.2478026>.
- [38] J. Dréon, et al., 23.5%-efficient silicon heterojunction silicon solar cell using molybdenum oxide as hole-selective contact, *Nano Energy* 70 (2020), 104495, <https://doi.org/10.1016/j.nanoen.2020.104495>.
- [39] J. Bullock, D. Yan, A. Cuevas, Y. Wan, C. Samundsett, N- and p-typesilicon solar cells with molybdenum oxide hole contacts, *Energy Procedia* 77 (2015) 446–450, <https://doi.org/10.1016/j.egypro.2015.07.063>.
- [40] H. Mehmood, H. Nasser, T. Tauqueer, R. Turan, Simulation of silicon heterostructure solar cell featuring dopant-free carrier-selective molybdenum oxide and titanium oxide contacts, *Renew. Energy* 143 (2019) 359–367.
- [41] X. Yang, K. Weber, Z. Hameiri, S.D. Wolf, Industrially feasible, dopant-free, carrier-selective contacts for high-efficiency silicon solar cells, *Prog. Photovolt. Res. Appl.* 25 (11) (2017) 896–904, <https://doi.org/10.1002/pip.2901>.
- [42] V. Titova, J. Schmidt, Selectivity of TiO<sub>x</sub>-based electron-selective contacts on n-type crystalline silicon and solar cell efficiency potential, *Phys. Status Solidi - Rapid Res. Lett.* 15 (9) (2021) 1–8, <https://doi.org/10.1002/pssr.202100246>.
- [43] Z. Yang, H. Lin, K.W.A. Chee, P. Gao, J. Ye, The role of front-surface charges in interdigitated back contact silicon heterojunction solar cells, *Nano Energy* 61 (2019) 221–227, <https://doi.org/10.1016/j.nanoen.2019.04.001>.
- [44] K. Masuko, et al., Achievement of more than 25% conversion efficiency with crystalline silicon heterojunction solar cell, *IEEE J. Photovolt.* 4 (6) (2014) 1433–1435, <https://doi.org/10.1109/JPHOTOV.2014.2352151>.
- [45] F. Haase, et al., Laser contact openings for local poly-Si-metal contacts enabling 26.1%-efficient POLO-IBC solar cells, *Sol. Energy Mater. Sol. Cells* 186 (2018) 184–193, <https://doi.org/10.1016/j.solmat.2018.06.020>.
- [46] C. Hollermann, et al., Separating the two polarities of the POLO contacts of an 26.1%-efficient IBC solar cell, *Sci. Rep.* 10 (1) (2020) 1–15, <https://doi.org/10.1038/s41598-019-57310-0>.
- [47] K. Yoshikawa, et al., Exceeding conversion efficiency of 26% by heterojunction interdigitated back contact solar cell with thin film Si technology, *Sol. Energy Mater. Sol. Cells* 173 (2017) 37–42, <https://doi.org/10.1016/j.solmat.2017.06.024>.
- [48] A. Richter et al., Both Sides Contacted Silicon Solar Cells: Options for Approaching 26% Efficiency in 36th European PV Solar Energy Conference and Exhibition, 2019, pp. 9–13. doi:10.4229/EUPVSEC20192019-2BP.1.3.
- [49] J.E. Cotter, J.H. Guo, P.J. Cousins, M.D. Abbott, F.W. Chen, K.C. Fisher, P-type versus n-type silicon wafers: prospects for high-efficiency commercial silicon solar cells, *IEEE Trans. Electron Devices* 53 (8) (2006) 1893–1901, <https://doi.org/10.1109/TED.2006.878026>.
- [50] D. Macdonald, L.J. Geerligs, Recombination activity of interstitial iron and other transition metal point defects in p- and n-type crystalline silicon, *Appl. Phys. Lett.* 85 (18) (2004) 4061–4063, <https://doi.org/10.1063/1.1812833>.
- [51] S.W. Glunz, S. Rein, J.Y. Lee, W. Warta, Minority carrier lifetime degradation in boron-doped Czochralski silicon, *J. Appl. Phys.* 90 (5) (2001) 2397–2404, <https://doi.org/10.1063/1.1389076>.
- [52] J. Schmidt, K. Bothe, Structure and transformation of the metastable boron- and oxygen-related defect center in crystalline silicon, *Phys. Rev. B* 69 (2) (2004) 24107, <https://doi.org/10.1103/PhysRevB.69.024107>.
- [53] S. Li, et al., Poly-Si/SiO<sub>x</sub>/c-Si passivating contact with 738 mV implied open circuit voltage fabricated by hot-wire chemical vapor deposition, *Appl. Phys. Lett.* 114 (15) (2019), 153901, <https://doi.org/10.1063/1.5089650>.
- [54] H. Park, et al., Passivation quality control in poly-Si/SiO<sub>x</sub>/c-Si passivated contact solar cells with 734 mV implied open circuit voltage, *Sol. Energy Mater. Sol. Cells* 189 (2019) 21–26, <https://doi.org/10.1016/j.solmat.2018.09.013>.
- [55] M. Bivour, J. Temmler, H. Steinke, M. Hermle, Molybdenum and tungsten oxide: high work function wide band gap contact materials for hole selective contacts of silicon solar cells, *Sol. Energy Mater. Sol. Cells* 142 (2015) 34–41, <https://doi.org/10.1016/j.solmat.2015.05.031>.
- [56] L.G. Gerling, et al., Transition metal oxides as hole-selective contacts in silicon heterojunctions solar cells, *Sol. Energy Mater. Sol. Cells* 145 (2) (2016) 109–115, <https://doi.org/10.1016/j.solmat.2015.08.028>.
- [57] Z. Wang, et al., Hole selective materials and device structures of heterojunction solar cells: recent assessment and future trends, *APL Mater.* 7 (11) (2019), 110701, <https://doi.org/10.1063/1.5121327>.
- [58] G. Sahasrabudhe, et al., Low-temperature synthesis of a TiO<sub>2</sub>/Si heterojunction, *J. Am. Chem. Soc.* 137 (2015) 14842–14845, <https://doi.org/10.1021/jacs.5b09750>.
- [59] Y. Wan, et al., Magnesium fluoride electron-selective contacts for crystalline silicon solar cells, *ACS Appl. Mater. Interface* 8 (23) (2016) 14671–14677, <https://doi.org/10.1021/acsami.6b03599>.
- [60] Y. Wan, et al., Conductive and stable magnesium oxide electron-selective contacts for efficient silicon solar cells, *Adv. Energy Mater.* 7 (5) (2017), 1601863, <https://doi.org/10.1002/aenm.201601863>.
- [61] L. He, C. Jiang, Rusli D. Lai, H. Wang, Highly efficient Si-nanorods/organic hybrid core-sheath heterojunction solar cells, *Appl. Phys. Lett.* 99 (2) (2011), <https://doi.org/10.1063/1.3610461>.
- [62] P. Yu, et al., 13% efficiency hybrid organic/silicon-nanowire heterojunction solar cell via interface engineering, *ACS Nano* 7 (12) (2013) 10780–10787, <https://doi.org/10.1021/nm403982b>.
- [63] D. Zielke, A. Pazidis, F. Werner, J. Schmidt, Organic-silicon heterojunction solar cells on n-type silicon wafers: the back PEDOT concept, *Sol. Energy Mater. Sol. Cells* 131 (2014) 110–116, <https://doi.org/10.1016/j.solmat.2014.05.022>.
- [64] Y.-C. Tseng, A.U. Mane, J.W. Elam, S.B. Darling, Ultrathin molybdenum oxide anode buffer layer for organic photovoltaic cells formed using atomic layer deposition, *Sol. Energy Mater. Sol. Cells* 99 (2012) 235–239, <https://doi.org/10.1016/j.solmat.2011.12.004>.
- [65] W. Wu, et al., Dopant-free back contact silicon heterojunction solar cells employing transition metal oxide emitters, *Phys. Status Solidi – Rapid Res. Lett.* vol. 10 (9) (2016) 662–667, <https://doi.org/10.1002/pssr.201600254>.
- [66] L.G. Gerling, C. Voz, R. Alcubilla, J. Puigdollers, Origin of passivation in hole-selective transition metal oxides for crystalline silicon heterojunction solar cells, *J. Mater. Res.* 32 (2) (2017) 260–268, <https://doi.org/10.1557/jmr.2016.453>.
- [67] M. Xue, et al., “Investigation of Nickel Oxide as Carrier-selective Interlayer for Silicon Solar Cell Contacts,” in 2018 IEEE 7th World Conference on Photovoltaic Energy Conversion (WCPEC) (A Joint Conference of 45th IEEE PVSC, 28th PVSEC & 34th EU PVSEC), 2018, pp. 2180–2182, doi:10.1109/PVSC.2018.8547476.
- [68] G. Masmitjà, et al., Interdigitated back-contacted crystalline silicon solar cells with low-temperature dopant-free selective contacts, *J. Mater. Chem. A* 6 (9) (2018) 3977–3985, <https://doi.org/10.1039/C7TA11308K>.
- [69] X. Yang, et al., Atomic layer deposition of vanadium oxide as hole-selective contact for crystalline silicon solar cells, *Adv. Electron. Mater.* 6 (8) (2020), <https://doi.org/10.1002/aelm.202000467>.
- [70] L.G. Gerling, G. Masmitja, P. Ortega, C. Voz, R. Alcubilla, J. Puigdollers, Passivating/hole-selective contacts based on V<sub>2</sub>O<sub>5</sub>/SiO<sub>x</sub> stacks deposited at ambient temperature, *Energy Procedia* 124 (2017) 584–592, <https://doi.org/10.1016/j.egypro.2017.09.294>.
- [71] E.R. Costals, et al., Atomic layer deposition of vanadium oxide films for crystalline silicon solar cells, *Mater. Adv.* (2022), <https://doi.org/10.1039/DIMA00812A>.
- [72] M. Bivour, J. Temmler, F. Zähringer, S. Glunz, and M. Hermle, “High work function metal oxides for the hole contact of silicon solar cells,” in 2016 IEEE 43rd Photovoltaic Specialists Conference (PVSC), 2016, pp. 0215–0220. doi:10.1109/PVSC.2016.7749581.

- [73] B. Macco, M.F.J. Vos, N.F.W. Thissen, A.A. Bol, W.M.M. Kessels, Low-temperature atomic layer deposition of MoO<sub>x</sub> for silicon heterojunction solar cells, *Phys. Status Solidi Res. Lett.* 9 (7) (2015) 393–396, <https://doi.org/10.1002/pssr.201510117>.
- [74] Y. Zhao, A.M. Nardes, K. Zhu, Effective hole extraction using MoO<sub>x</sub>–Al contact in perovskite CH<sub>3</sub>NH<sub>3</sub>PbI<sub>3</sub> solar cells, *Appl. Phys. Lett.* 104 (213906) (2014), <https://doi.org/10.1063/1.4880899>.
- [75] C. Battaglia, S.M. Nicolás, S.D. Wolf, X. Yin, M. Zheng, C. Ballif, Silicon heterojunction solar cell with passivated hole selective MoO<sub>x</sub> contact, *Appl. Phys. Lett.* 104 (2014), 113902, <https://doi.org/10.1063/1.4868880>.
- [76] J. Bullock, et al., Efficient silicon solar cells with dopant-free asymmetric heterocontacts, *Nat. Energy* 1 (2016) 15031, <https://doi.org/10.1038/nenergy.2015.31>.
- [77] H. Dai, L. Yang, S. He, <50-μm thin crystalline silicon heterojunction solar cells with dopant-free carrier-selective contacts, *Nano Energy* 64 (2019), 103930, <https://doi.org/10.1016/j.nanoen.2019.103930>.
- [78] S. Avasthi, W.E. McClain, G. Man, A. Kahn, J. Schwartz, J.C. Sturm, Hole-blocking titanium-oxide/silicon heterojunction and its application to photovoltaics, *Appl. Phys. Lett.* 102 (2013), 203901, <https://doi.org/10.1063/1.4803446>.
- [79] J. Cho, et al., Thermal stability improvement of metal oxide-based contacts for silicon heterojunction solar cells, *Sol. Energy Mater. Sol. Cells* 206 (2020), 110324, <https://doi.org/10.1016/j.solmat.2019.110324>.
- [80] X. Yang, Q. Bi, H. Ali, K. Davis, W.V. Schoenfeld, K. Weber, High-performance TiO<sub>2</sub>-based electron-selective contacts for crystalline silicon solar cells, *Adv. Mater.* 28 (28) (2016) 5891–5897, <https://doi.org/10.1002/adma.201600926>.
- [81] M. Boccard, X. Yang, K. Weber, Z.C. Holman, Passivation and Carrier Selectivity of TiO<sub>2</sub> Contacts Combined with Different Passivation Layers and Electrodes for Silicon Solar Cells, 2016 IEEE 43rd Photovoltaic Specialists Conference, PVSC 2016, United States, 2016, pp. 2403–2407, <https://doi.org/10.1109/PVSC.2016.7750072>.
- [82] N. Mozaffari, et al., Efficient passivation and low resistivity for p+-Si/TiO<sub>2</sub> contact by atomic layer deposition, *ACS Appl. Energy Mater.* 3 (7) (2020) 6291–6301, <https://doi.org/10.1021/acsena.0c00378>.
- [83] J. Cho, et al., Passivating electron-selective contacts for silicon solar cells based on an a-Si:H/TiOx stack and a low work function metal, *Prog. Photovolt. Res. Appl.* 26 (10) (2018) 835–845, <https://doi.org/10.1002/pip.3023>.
- [84] B. Liao, B. Hoex, A.G. Aberle, D. Chi, C.S. Bhatia, Excellent c-Si surface passivation by low-temperature atomic layer deposited titanium oxide, *Appl. Phys. Lett.* 104 (25) (2014), 253903, <https://doi.org/10.1063/1.4885096>.
- [85] L. Chen, et al., 14.1% efficiency hybrid planar-Si/organic heterojunction solar cells with SnO<sub>2</sub> insertion layer, *Sol. Energy* 174 (2018) 549–555, <https://doi.org/10.1016/j.solener.2018.09.035>.
- [86] Y. Zheng, et al., Optimization of SnO<sub>2</sub>-based electron-selective contacts for Si/PEDOT:PSS heterojunction solar cells, *Sol. Energy* 193 (2019) 502–506, <https://doi.org/10.1016/j.solener.2019.09.077>.
- [87] Y. Wan, et al., Tantalum oxide electron-selective heterocontacts for silicon photovoltaics and photoelectrochemical water reduction, *ACS Energy Lett.* 3 (1) (2018) 125–131, <https://doi.org/10.1021/acsenergylett.7b01153>.
- [88] J. Bullock, et al., Dopant-free partial rear contacts enabling 23% silicon solar cells, *Adv. Energy Mater.* 9 (9) (2019) 1–6, <https://doi.org/10.1002/aenm.201803367>.
- [89] Z.Q. Ma, B. He, TCO-Si Based Heterojunction Photovoltaic Devices. Solar Cells - Thin-Film Technologies, IntechOpen, 2011, pp. 111–137. <https://www.intechopen.com/chapters/22803>.
- [90] G. Brauer, J. Kuripach, C.C. Ling, A.B. Djurisic, Activities towards p-type doping of ZnO, *J. Phys. Conf. Ser.* 265 (12002) (2011), <https://doi.org/10.1088/1742-6596/265/1/012002>.
- [91] A. Klein, et al., Transparent conducting oxides for photovoltaics: Manipulation of fermi level, work function and energy band alignment, *Material* 3 (11) (2010) 4892–4914, <https://doi.org/10.3390/ma3114892>.
- [92] C. Luderer, L. Tutsch, C. Messmer, M. Hermle, M. Bivour, Influence of TCO and a-Si:H doping on SHJ contact resistivity, *IEEE J. Photovolt.* 11 (2) (2021) 329–336, <https://doi.org/10.1109/JPHOTOV.2021.3051206>.
- [93] R. Saive, et al., Silicon heterojunction solar cells with effectively transparent front contacts, *Sustain. Energy Fuels* 1 (3) (2017) 593–598, <https://doi.org/10.1039/C7SE00096K>.
- [94] M. Singh, P. Prasher, J. Kim, Solution processed silver-nanowire/zinc oxide based transparent conductive electrode for efficient photovoltaic performance, *Nano-Struct. Nano-Objects* 16 (2018) 151–155, <https://doi.org/10.1039/C3NR00863K>.
- [95] M. Bivour, S. Schröer, M. Hermle, Numerical analysis of electrical TCO/a-Si: H (p) contact properties for silicon heterojunction solar cells, *Energy Procedia* 38 (2013) 658–669, <https://doi.org/10.1016/j.egypro.2013.07.330>.
- [96] C. Battaglia, A. Cuevas, S. De Wolf, High-efficiency crystalline silicon solar cells: status and perspectives, *Energy Environ. Sci.* 9 (5) (2016) 1552–1576, <https://doi.org/10.1039/C5EE03380B>.
- [97] P. Kuang, et al., A new architecture for transparent electrodes: relieving the trade-off between electrical conductivity and optical transmittance, *Adv. Mater.* 23 (21) (2011) 2469–2473, <https://doi.org/10.1002/adma.201100419>.
- [98] J. van de Groep, P. Spinelli, A. Polman, Transparent Conducting Silver Nanowire Networks, *Nano Lett.* 12 (6) (2012) 3138–3144, <https://doi.org/10.1021/nl301045a>.
- [99] Y. Zang, et al., Graphene as transparent electrode in Si solar cells: a dry transfer method, *AIP Adv.* 8 (6) (2018) 65206, <https://doi.org/10.1063/1.5030571>.
- [100] L. Lancellotti, et al., Graphene as non conventional transparent conductive electrode in silicon heterojunction solar cells, *Appl. Surf. Sci.* 525 (p. 146443) (2020), <https://doi.org/10.1016/j.apsusc.2020.146443>.
- [101] S. Das, D. Pandey, J. Thomas, T. Roy, The role of graphene and Other 2D materials in solar photovoltaics, *Adv. Mater.* 31 (1) (2019), 1802722, <https://doi.org/10.1002/adma.201802722>.
- [102] M. Morales-Masis, S. De Wolf, R. Woods-Robinson, J.W. Ager, C. Ballif, Transparent electrodes for efficient optoelectronics, *Adv. Electron. Mater.* 3 (5) (2017), 1600529, <https://doi.org/10.1002/aem.201600529>.
- [103] T. Mueller, S. Schwertheim, M. Scherff, W.R. Fahrner, High quality passivation for heterojunction solar cells by hydrogenated amorphous silicon suboxide films, *Appl. Phys. Lett.* 92 (3) (2008) 33504, <https://doi.org/10.1063/1.2837192>.
- [104] L. Mazzarella, S. Kirner, B. Stannowski, L. Korte, B. Rech, R. Schlattmann, p-type microcrystalline silicon oxide emitter for silicon heterojunction solar cells allowing current densities above 40 mA/cm<sup>2</sup>, *Appl. Phys. Lett.* 106 (2) (2015) 23902, <https://doi.org/10.1063/1.4905906>.
- [105] J. Peter Seif, et al., Amorphous silicon oxide window layers for high-efficiency silicon heterojunction solar cells, *J. Appl. Phys.* 115 (2) (2014) 24502, <https://doi.org/10.1063/1.4861404>.
- [106] H. Fujiwara, T. Kaneko, M. Kondo, Application of hydrogenated amorphous silicon oxide layers to c-Si heterojunction solar cells, *Appl. Phys. Lett.* 91 (13) (2007), 133508, <https://doi.org/10.1063/1.2790815>.
- [107] T. Mueller, W. Duengen, Y. Ma, R. Job, M. Scherff, W.R. Fahrner, Investigation of the emitter band gap widening of heterojunction solar cells by use of hydrogenated amorphous carbon silicon alloys, *J. Appl. Phys.* 102 (7) (2007) 74505, <https://doi.org/10.1063/1.2785012>.
- [108] M. Boccard, Z.C. Holman, Amorphous silicon carbide passivating layers for crystalline-silicon-based heterojunction solar cells, *J. Appl. Phys.* 118 (6) (2015) 65704, <https://doi.org/10.1063/1.4928203>.
- [109] Z.C. Holman, A. Descoedures, S. De Wolf, C. Ballif, Record infrared internal quantum efficiency in silicon heterojunction solar cells with dielectric/metal rear reflectors, *IEEE J. Photovolt.* 3 (4) (2013) 1243–1249, <https://doi.org/10.1109/JPHOTOV.2013.2276484>.
- [110] M. Otto, et al., Conformal transparent conducting oxides on black silicon, *Adv. Mater.* 22 (44) (2010) 5035–5038, <https://doi.org/10.1002/adma.201002515>.
- [111] J. Bullock, et al., Amorphous silicon passivated contacts for diffused junction silicon solar cells, *J. Appl. Phys.* 115 (16) (2014), 163703, <https://doi.org/10.1063/1.4872262>.
- [112] W.K. Oh, S.Q. Hussain, Y.J. Lee, Y. Lee, S. Ahn, J. Yi, Study on the ITO work function and hole injection barrier at the interface of ITO/a-Si:H(p) in amorphous/crystalline silicon heterojunction solar cells, *Mater. Res. Bull.* 47 (10) (2012) 3032–3035, <https://doi.org/10.1016/j.materresbull.2012.04.106>.
- [113] Y.S. Park, E. Kim, B. Hong, J. Lee, Characteristics of ITO films with oxygen plasma treatment for thin film solar cell applications, *Mater. Res. Bull.* 48 (12) (2013) 5115–5120, <https://doi.org/10.1016/j.materresbull.2013.07.026>.
- [114] M. Kim, J. Kim, J. Cho, H. Kim, N. Lee, B. Choi, A study of the characteristics of indium tin oxide after chlorine electro-chemical treatment, *Mater. Res. Bull.* 82 (2016) 115–121, <https://doi.org/10.1016/j.materresbull.2016.03.008>.
- [115] O. Madani Ghahfarokhi, K. Chakanga, S. Geissendoerfer, O. Sergeev, K. von Maydell, C. Agert, DC-sputtered ZnO:Al as transparent conductive oxide for silicon heterojunction solar cells with μc-Si:H emitter, *Prog. Photovolt. Res. Appl.* 23 (10) (2015) 1340–1352, <https://doi.org/10.1002/pip.2570>.
- [116] S. Kim, et al., Role of double ITO/In<sub>2</sub>O<sub>3</sub> layer for high efficiency amorphous/crystalline silicon heterojunction solar cells, *Mater. Res. Bull.* 58 (2014) 83–87, <https://doi.org/10.1016/j.materresbull.2014.05.003>.
- [117] J. Shi, et al., MoO<sub>x</sub> modified ITO/a-Si:H(p) contact for silicon heterojunction solar cell application, *Mater. Res. Bull.* 97 (2017) (2018) 176–181, <https://doi.org/10.1016/j.materresbull.2017.09.005>.
- [118] J. Bullock, D. Yan, A. Cuevas, Y. Wan, C. Samundsett, N-and p-type silicon solar cells with molybdenum oxide hole contacts, *Energy Procedia* 77 (2015) 446–450, <https://doi.org/10.1016/j.egypro.2015.07.063>.
- [119] J. Geissbühler, et al., 22.5% efficient silicon heterojunction solar cell with molybdenum oxide hole collector, *Appl. Phys. Lett.* 107 (8) (2015) 81601, <https://doi.org/10.1063/1.4928747>.
- [120] Z. Yang, P. Gao, J. Sheng, H. Tong, C. Quan, X. Yang, K.W.A. Chee, B. Yan, Y. Zeng, J. Ye, Principles of dopant-free electron-selective contacts based on tunnel oxide/low work-function metal stacks and their applications in heterojunction solar cells, *Nano Energy* 46 (2018) 133–140, <https://doi.org/10.1016/j.nanoen.2018.01.043>.
- [121] J. Bullock (2016) Advanced Contacts for crystalline silicon solar cells, PhD thesis, Australian National University. Available: <https://openresearch-repository.anu.edu.au/handle/1885/110957>. Accessed Sept. 15, 2020.
- [122] S. Duttagupta, F. Lin, K.D. Shetty, A.G. Aberle, B. Hoex, Excellent boron emitter passivation for high-efficiency Si wafer solar cells using AlO<sub>x</sub>/SiNx dielectric stacks deposited in an industrial inline plasma reactor, *Prog. Photovolt. Res. Appl.* 21 (4) (2013) 760–764, <https://doi.org/10.1002/pip.1259>.
- [123] G. Lu, F. Zheng, J. Wang, W. Shen, Thin Al<sub>2</sub>O<sub>3</sub> passivated boron emitter of n-type bifacial c-Si solar cells with industrial process, *Prog. Photovolt. Res. Appl.* 25 (4) (2017) 280–290, <https://doi.org/10.1002/pip.2859>.
- [124] K.A. Collett, M. Cyron, R.S. Bonilla, P.R. Wilshaw, Surface Passivation Provided by an Alneal through SiO<sub>2</sub>/TiO<sub>2</sub> Bilayer, Proceedings of the 32nd Eur. Photovolt. Sol. Energy Conf. Exhib., Munich, Germany (2016) 811–815, <https://doi.org/10.4229/EUPVSEC20162016-2AV.3.20>.

- [125] C. Lee, et al., Properties of thermally evaporated titanium dioxide as an electron-selective contact for silicon solar cells, *Energies* 13 (3) (2020), 678, <https://doi.org/10.3390/en13030678>.
- [126] C. Battaglia, et al., Hole selective MoO<sub>x</sub> contact for silicon solar cells, *Nano Lett.* 14 (2) (2014) 967–971, <https://doi.org/10.1021/nl404389u>.
- [127] H.-D. Um, N. Kim, K. Lee, I. Hwang, J.H. Seo, K. Seo, Dopant-free all-back-contact Si nanohole solar cells using MoO<sub>x</sub> and LiF films, *Nano Lett.* 16 (2016) 981–987, <https://doi.org/10.1021/acs.nanolett.5b03955>.
- [128] J. Bullock, A. Cuevas, T. Allen, C. Battaglia, Molybdenum oxide MoO<sub>x</sub>: a versatile hole contact for silicon solar cells, *Appl. Phys. Lett.* 105 (23) (2014), 232109, <https://doi.org/10.1063/1.4903467>.
- [129] A. Paduthol, M.K. Juhl, G. Nogay, P. Löper, A. Ingenito, and T. Trupke, “Carrier injection from amorphous silicon into crystalline silicon determined with photoluminescence,” in 2018 IEEE 7th World Conference on Photovoltaic Energy Conversion (WCPEC)(A Joint Conference of 45th IEEE PVSC, 28th PVSEC & 34th EU PVSEC), 2018, pp. 3746–3750. doi:10.1109/PVSC.2018.8547295.
- [130] A. Paduthol, M.K. Juhl, G. Nogay, P. Löper, T. Trupke, Measuring carrier injection from amorphous silicon into crystalline silicon using photoluminescence, *Prog. Photovolt. Res. Appl.* 26 (12) (2018) 968–973, <https://doi.org/10.1002/pip.3042>.
- [131] K.A. Gesheva, A. Cziraki, T. Ivanova, A. Szekeres, Crystallization of chemicallyvapor deposited molybdenum and mixed tungsten/molybdenum oxide filmsfor electrochromic application, *Thin Solid Films* 515 (2007) 4609–4613, <https://doi.org/10.1016/j.tsf.2006.11.042>.
- [132] R. Sivakumar, R. Gopalakrishnan, M. Jayachandran, C. Sanjeeviraja, Characterization on electron beam evaporated a-MoO<sub>3</sub> thin films by the influence of substrate temperature, *Curr. Appl. Phys.* 7 (1) (2007) 51–59, <https://doi.org/10.1016/j.cap.2005.10.001>.
- [133] S.H. Mohamed, S. Venkataraj, Thermal stability of amorphous molybdenumtrioxide films prepared at different oxygen partial pressures by reactive DC magnetron sputtering, *Vacuum* 81 (2007) 636–643, <https://doi.org/10.1016/j.vacuum.2006.08.006>.
- [134] S.K. Deb, J.A. Chopoorian, Optical properties and color-center formation in thin films of molybdenum trioxide, *J. Appl. Phys.* 37 (13) (1966) 4818–4825, <https://doi.org/10.1063/1.1708145>.
- [135] M.S. Jagadeesh, D. V.D, Colour centre studies in MoO<sub>3</sub> films, *J. Non Cryst. Solids* 28 (3) (1978) 327–335, [https://doi.org/10.1016/0022-3093\(78\)90084-4](https://doi.org/10.1016/0022-3093(78)90084-4).
- [136] N. Miyata, T. Suzuki, R. Ohyama, Physical properties of evaporated molybdenum oxide films, *Thin Solid Films* 281 (1996) 218–222, [https://doi.org/10.1016/0040-6090\(96\)08617-8](https://doi.org/10.1016/0040-6090(96)08617-8).
- [137] T. Siciliano, A. Tepore, E. Filippo, G. Micocci, M. Tepore, Characteristics of molybdenum trioxide nanobelts prepared by thermal evaporation technique, *Mater. Chem. Phys.* 114 (2009) 687–691, <https://doi.org/10.1016/j.matchemphys.2008.10.018>.
- [138] S. McDonnell, et al., Hole contacts on transition metal dichalcogenides:interface chemistry and band alignments, *ACS Nano* 8 (6) (2014) 6265–6272, <https://doi.org/10.1021/nn501728w>.
- [139] E. Bobeico, et al., Evaporated MoO<sub>x</sub> as general back-side hole collector for solar cells, *Coatings* 10 (8) (2020) 1–12, <https://doi.org/10.3390/COATINGS10080763>.
- [140] H. Mehmood, G. Bektaş, İ. Yıldız, T. Tauqeer, H. Nasser, R. Turan, Electrical, optical and surface characterization of reactive RF magnetron sputtered molybdenum oxide films for solar cell applications, *Mater. Sci. Semicond. Process.* 101 (2019) 46–56, <https://doi.org/10.1016/j.mssp.2019.05.018>.
- [141] J. Tong, Y. Wan, J. Cui, S. Lim, N. Song, A. Lennon, Solution-processed molybdenum oxide for hole-selective contacts on crystalline silicon solar cells, *Appl. Surf. Sci.* 423 (2017) 139–146, <https://doi.org/10.1016/j.apsusc.2017.06.011>.
- [142] H. Mehmood, T. Tauqeer, H. Nasser, S. Hussain, R. Turan. Effect of hole-selective molybdenum oxide work function and silicon wafer resistivity on dopant-free asymmetric silicon heterostructure solar cell, *IEEE, Morocco*, 2017, pp. 1–5, <https://doi.org/10.1109/IRSEC.2017.8477335>.
- [143] K. Mallem, et al., Molybdenum oxide: a superior hole extraction layer for replacing p-type hydrogenated amorphous silicon with high efficiency heterojunction Si solar cells, *Mater. Res. Bull.* 110 (2019) 90–96, <https://doi.org/10.1016/j.materresbull.2018.10.018>.
- [144] J. Cho, et al., Interface analysis and intrinsic thermal stability of MoO<sub>x</sub> based hole-selective contacts for silicon heterojunction solar cells, *Sol. Energy Mater. Sol. Cells* 201 (2019), 110074, <https://doi.org/10.1016/j.solmat.2019.110074>.
- [145] S. Essig, et al., Toward annealing-stable molybdenum-oxide-based hole-selective contacts for silicon photovoltaics, *Sol. RRL* 2 (4) (2018), 1700227, <https://doi.org/10.1002/solr.201700227>.
- [146] D. Sacchetto, et al., ITO/MoO<sub>x</sub>/a-Si: H (i) hole-selective contacts for silicon heterojunction solar cells: degradation mechanisms and cell integration, *IEEE J. Photovolt.* 7 (6) (2017) 1584–1590, <https://doi.org/10.1109/JPHOTOV.2017.2756066>.
- [147] H. Ali, G. Gregory, M. Bivour, M. Schneider, M. Hermle, K.O. Davis, TEM studies of hole-selective molybdenum oxide contacts in silicon heterojunction solar cells, *Microsc. Microanal.* 24 (S1) (2018) 1508–1509, <https://doi.org/10.1017/S1431927618008024>.
- [148] H. Ali, et al., In situ transmission electron microscopy study of molybdenum oxide contacts for silicon solar cells, *Phys. Status Solidi* 1800998 (2019) 1–4, <https://doi.org/10.1002/pssa.201800998>.
- [149] K. Mallem et al., Influence of molybdenum oxide thickness, electronic structure, and work function on the performance of hole selective silicon heterojunction solar cells In 2019 26th International Workshop on Active-Matrix Flatpanel Displays and Devices (AM-FPD), Kyoto, Japan, 2019, pp. 1–4.doi: 10.23919/AM-FPD.2019.8830558.
- [150] M. Gao, et al., Effective passivation and tunneling hybrid a-SiO<sub>x</sub>(In) layer in ITO/n-Si heterojunction photovoltaic device, *ACS Appl. Mater. Interfaces* 9 (20) (2017) 17565–17575, <https://doi.org/10.1021/acsami.7b01447>.
- [151] X.M. Song, et al., Interface properties of ITO/n-Si heterojunction solar cell: quantum tunneling, passivation and hole-selective contacts, *Sol. Energy* 173 (2018) 456–461, <https://doi.org/10.1016/j.solener.2018.07.083>.
- [152] A. Louwen, W. Van Sark, R. Schropp, A. Faaij, A cost roadmap for silicon heterojunction solar cells, *Sol. Energy Mater. Sol. Cells* 147 (2016) 295–314, <https://doi.org/10.1016/j.solmat.2015.12.026>.
- [153] M. Nicolai, M. Zanuccoli, F. Feldmann, M. Hermle, C. Fiegna, Analysis of silicon solar cells with poly-Si/SiO<sub>x</sub> carrier-selective base and emitter contacts, *IEEE J. Photovolt.* 8 (1) (2017) 103–109, <https://doi.org/10.1109/JPHOTOV.2017.2775142>.
- [154] A.B. Morales-Vilches, et al., ITO-free silicon heterojunction solar cells with ZnO: Al/SiO<sub>2</sub> front electrodes reaching a conversion efficiency of 23%, *IEEE J. Photovolt.* 9 (1) (2018) 34–39, <https://doi.org/10.1109/JPHOTOV.2018.2873307>.
- [155] L. Gong, C. Zhou, J. Zhu, W. Wang, Passivation characteristics of new silicon oxide, *IEEE J. Photovolt.* 9 (6) (2019) 1873–1879, <https://doi.org/10.1109/JPHOTOV.2019.2929445>.
- [156] H. Geng, et al., Advanced passivation techniques for Si solar cells with high- $\kappa$  dielectric materials, *Appl. Phys. Lett.* 105 (12) (2014), 123905, <https://doi.org/10.1063/1.4896619>.
- [157] J. John (Ed.), *Surface Passivation of Industrial Crystalline Silicon Solar Cells*, Institution of Engineering and Technology, London, U.K., 2018. <https://digital-library.theiet.org/content/books/po/pbpo106e>.
- [158] B.S. Richards, Comparison of TiO<sub>2</sub> and other dielectric coatings for buried-contact solar cells: a review, *Prog. Photovolt. Res. Appl.* 12 (4) (2004) 253–281, <https://doi.org/10.1002/pip.529>.
- [159] B. Sopori, Dielectric films for Si solar cell applications, *J. Electron. Mater.* 34 (5) (2005) 564–570, <https://doi.org/10.1007/s11664-005-0066-9>.
- [160] J. Schmidt, et al., Advances in the surface passivation of silicon solar cells, *Energy Procedia* 15 (2012) 30–39, <https://doi.org/10.1016/j.egypro.2012.02.004>.
- [161] S. Zhong, et al., Mitigating plasmonic absorption losses at rear electrodes in high-efficiency silicon solar cells using dopant-free contact stacks, *Adv. Funct. Mater.* 30 (5) (2020) 1–9, <https://doi.org/10.1002/adfm.201907840>.
- [162] K. Yamamoto, K. Yoshikawa, H. Uzu, D. Adachi, High-efficiency heterojunction crystalline Si solar cells, *Jpn. J. Appl. Phys.* 57 (8S3) (2018), 08RB20, <https://doi.org/10.7567/JJAP.57.08RB20>.
- [163] Y.F. Zhuang, S.H. Zhong, X.J. Liang, H.J. Kang, Z.P. Li, W.Z. Shen, Application of SiO<sub>2</sub> passivation technique in mass production of silicon solar cells, *Sol. Energy Mater. Sol. Cells* 193 (2019) 379–386, <https://doi.org/10.1016/j.solmat.2019.01.038>.
- [164] T.N. Truong, et al., Hydrogenation mechanisms of poly-Si/SiO<sub>x</sub> passivating contacts by different capping layers, *Sol. RRL* 4 (3) (2020), 1900476, <https://doi.org/10.1002/solr.201900476>.
- [165] Z.P. Ling, Z. Xin, P. Wang, R. Sridharan, C. Ke, R. Stangl, Double-Sided Passivated Contacts for Solar Cell Applications: An Industrially Viable Approach Toward 24% Efficient Large Area Silicon Solar Cells in *Silicon Materials*, IntechOpen (2019), <https://doi.org/10.5772/intechopen.85039>.
- [166] T. Gao, et al., An industrially viable TOPCon structure with both ultra-thin SiO<sub>x</sub> and n+-poly-Si processed by PECVD for p-type c-Si solar cells, *Sol. Energy Mater. Sol. Cells* 200 (2019), 109926, <https://doi.org/10.1016/J.SOLMAT.2019.109926>.
- [167] Y. Chen, et al., Mass production of industrial tunnel oxide passivated contacts (i-TOPCon) silicon solar cells with average efficiency over 23% and modules over 345 W, *Prog. Photovolt. Res. Appl.* 27 (10) (2019) 827–834, <https://doi.org/10.1002/pip.3180>.
- [168] D. Chen, et al., 24.58% total area efficiency of screen-printed, large area industrial silicon solar cells with the tunnel oxide passivated contacts (i-TOPCon) design, *Sol. Energy Mater. Sol. Cells* 206 (2020), 110258, <https://doi.org/10.1016/j.solmat.2019.110258>.
- [169] Q. Wang, W. Wu, N. Yuan, Y. Li, Y. Zhang, J. Ding, Influence of SiO<sub>x</sub> film thickness on electrical performance and efficiency of TOPCon solar cells, *Sol. Energy Mater. Sol. Cells* 208 (2020), 110423, <https://doi.org/10.1016/j.solmat.2020.110423>.
- [170] M.A. Green, Photovoltaic technology and visions for the future, *Prog. Energy* 1 (1) (2019), 013001, <https://doi.org/10.1088/2516-1083/ab0fa8>.
- [171] H. Park, et al., Role of polysilicon in poly-Si/SiO<sub>x</sub> passivating contacts for high-efficiency silicon solar cells, *RSC Adv.* 9 (40) (2019) 23261–23266, <https://doi.org/10.1039/C9RA03560E>.
- [172] A. Moldovan, F. Feldmann, M. Zimmer, J. Rentsch, J. Benick, M. Hermle, Tunnel oxide passivated carrier-selective contacts based on ultra-thin SiO<sub>2</sub> layers, *Sol. Energy Mater. Sol. Cells* 142 (2015) 123–127, <https://doi.org/10.1016/J.SOLMAT.2015.06.048>.
- [173] R. van der Vossen, F. Feldmann, A. Moldovan, M. Hermle, Comparative study of differently grown tunnel oxides for p-type passivating contacts, *Energy Procedia* 124 (2017) 448–454, <https://doi.org/10.1016/j.egypro.2017.09.273>.
- [174] T.S. Yadav, A.K. Sharma, A. Kottantharayil, P.K. Basu, Comparative study of different silicon oxides used as interfacial passivation layer (SiNy: H/SiO<sub>x</sub>/n+-Si) in industrial monocrystalline silicon solar cells, *Sol. Energy Mater. Sol. Cells* 201 (1) (2019), 110077, <https://doi.org/10.1016/j.solmat.2019.110077>.
- [175] T.S. Yadav, A.K. Sharma, A. Kottantharayil, P.K. Basu, Low-cost and low-temperature chemical oxide passivation process for large area single crystalline

- silicon solar cells, Sol. Energy 169 (2018) 270–276, <https://doi.org/10.1016/j.solener.2018.04.008>.
- [176] W. Chen, R. Liu, Q. Zeng, L. Zhou, Low cost multicrystalline bifacial PERC solar cells—Fabrication and thermal improvement, Sol. Energy 184 (2019) 508–514, <https://doi.org/10.1016/j.solener.2019.04.033>.
- [177] Y. Li, et al., Optical and electrical performance of rear side epitaxial emitters for bifacial silicon solar cell application, Sol. Energy Mater. Sol. Cells 195 (2019) 43–48, <https://doi.org/10.1016/j.solmat.2019.01.051>.
- [178] G. Kaur, et al., Understanding surface treatment and ALD AlO<sub>x</sub> thickness induced surface passivation quality of c-Si Cz wafers, IEEE J. Photovolt. 7 (5) (2017) 1224–1235, <https://doi.org/10.1109/JPHOTOV.2017.2717040>.
- [179] L. Gong, C. Zhou, J. Zhu, W. Wang, and F. Ji, “Passivation Mechanisms of Atomic Layer-deposited AlO<sub>x</sub> Films and AlO<sub>x</sub>/SiO<sub>x</sub> Stack,” IOP Conf. Ser. Mater. Sci. Eng., vol. 585, no. 1, p. 012026, 2019.
- [180] A. Laades, et al., On the impact of interfacial SiO<sub>x</sub>-layer on the passivation properties of PECVD synthesized aluminum oxide, Phys. Status Solidi 9 (10–11) (2012) 2120–2123, <https://doi.org/10.1002/pssc.201200244>.
- [181] R.M. Swanson, P.J. Verlinden, and R.A. Sinton, “Method of making a solar cell having improved anti-reflection passivation layer,” U.S. Patent 5907766, May 25, 1999. Available: <https://patents.google.com/patent/US5907766A>, Accessed Oct. 12, 2020.
- [182] M. Hayes, B. Martel, S. Dubois, A. Morisset, O. Palais, Study of non fire-through metallization processes of boron-doped polysilicon passivated contacts for high efficiency silicon solar cells, AIP Conf. Proc. 2147 (1) (2019) 40006, <https://doi.org/10.1063/1.5123833>.
- [183] M. Stodolny et al., “PolySi Based Passivating Contacts Enabling Industrial Silicon Solar Cell Efficiencies up to 24%,” in 2019 IEEE 46th Photovoltaic Specialists Conference (PVSC), 2019, Chicago, IL, USA. pp. 1456–1459. doi: 10.1109/PVSC40753.2019.8980806.
- [184] Y. Larionova, et al., On the recombination behavior of p+-type polysilicon on oxide junctions deposited by different methods on textured and planar surfaces, Phys. Status Solidi 214 (8) (2017), 1700058, <https://doi.org/10.1002/pssa.201700058>.
- [185] B. Nemeth, et al., Polycrystalline silicon passivated tunneling contacts for high efficiency silicon solar cells, J. Mater. Res. 31 (6) (2016) 671–681, <https://doi.org/10.1557/jmr.2016.77>.
- [186] M. Schnabel, et al., Hydrogen passivation of poly-Si/SiO<sub>x</sub> contacts for Si solar cells using Al<sub>2</sub>O<sub>3</sub> studied with deuterium, Appl. Phys. Lett. 112 (20) (2018), 203901, <https://doi.org/10.1063/1.5031118>.
- [187] M.K. Stodolny, et al., n-Type polysilicon passivating contact for industrial bifacial n-type solar cells, Sol. Energy Mater. Sol. Cells 158 (2016) 24–28, <https://doi.org/10.1016/j.solmat.2016.06.034>.
- [188] G. Nogay, et al., Interplay of annealing temperature and doping in hole selective rear contacts based on silicon-rich silicon-carbide thin films, Sol. Energy Mater. Sol. Cells 173 (2017) 18–24, <https://doi.org/10.1016/j.solmat.2017.06.039>.
- [189] G. Dingemans, W. Beyer, M.C.M. van de Sanden, W.M.M. Kessels, Hydrogen induced passivation of Si interfaces by Al<sub>2</sub>O<sub>3</sub> films and SiO<sub>2</sub>/Al<sub>2</sub>O<sub>3</sub> stacks, Appl. Phys. Lett. 97 (15) (2010), 152106, <https://doi.org/10.1063/1.3497014>.
- [190] B.W.H. van de Loo, et al., On the hydrogenation of poly-Si passivating contacts by Al<sub>2</sub>O<sub>3</sub> and SiN<sub>x</sub> thin films, Sol. Energy Mater. Sol. Cells 215 (2019) (2020), 110592, <https://doi.org/10.1016/j.solmat.2020.110592>.
- [191] L. Tutsch, F. Feldmann, B. Macco, M. Bivou, E. Kessels, M. Hermle, Improved passivation of n-type poly-Si based passivating contacts by the application of hydrogen-rich transparent conductive oxides, IEEE J. Photovolt. 10 (4) (2020) 986–991, <https://doi.org/10.1109/JPHOTOV.2020.2992348>.
- [192] A. Mewe, et al., Full wafer size IBC cell with polysilicon passivating contacts, AIP Conf. Proc. 1999 (1) (2018), 040014, <https://doi.org/10.1063/1.5049277>.
- [193] J. Schmidt, B. Veith, R. Brendel, Effective surface passivation of crystalline silicon using ultrathin Al<sub>2</sub>O<sub>3</sub> films and Al<sub>2</sub>O<sub>3</sub>/SiN<sub>x</sub> stacks, Phys. Status Solidi – Rapid Res. Lett. 3 (9) (2009) 287–289, <https://doi.org/10.1002/pssr.200903272>.
- [194] E. Bruhat, T. Desrues, D. Blanc-Pelissier, B. Martel, R. Cabal, S. Dubois, TCO contacts on poly-Si layers: High and low temperature approaches to maintain passivation and contact properties, AIP Conf. Proc. 2147 (1) (2019), 040001, <https://doi.org/10.1063/1.5123828>.
- [195] X. Yan, et al., Investigation of phosphorus diffused back surface field (BSF) in bifacial nFAB solar cells, Sol. Energy 179 (2019) 335–342, <https://doi.org/10.1016/j.solener.2018.12.052>.
- [196] J. Sheng, et al., Impact of phosphorus diffusion on n-type poly-Si based passivated contact silicon solar cells, Sol. Energy Mater. Sol. Cells 203 (2019), 110120, <https://doi.org/10.1016/j.solmat.2019.110120>.



**Dr. K.-W. A. Chee**, Ph.D, is a Professor, invited to Hefei on a talent program. He was a senior director in the electronics manufacturing industry, and public sector. Drawing from a rich industrial experience of product and technology development, his academic research currently investigates novel carrier-selective contacts for high-efficiency solar cells. He received prizes and awards from several bodies, including the Materials Research Society, U.S.A., the Chinese government (overseas scholar/talent programs), P. R. China, the Royal Academy of Engineering, IET, and IOP in the U.K., as well as the Cambridge Philosophical Society at which he is an elected Fellow.



**Dr. B. K. Ghosh** has received his Doctor of Engineering (DE) from Fukui University, Japan in Graduate School of Engineering in 2004 under Monbusho Scholarship. Currently he is working in Electrical and Electronic Engineering program under Faculty of Engineering in Universiti Malaysia Sabah, Malaysia as senior lecturer. His research area is solar PV materials, nano and opto-electronics. For higher opto-electrical gain emitter and TCO materials choice for hetero-junction (HJ) or HJ hybrid solar cell (HHSC) and suitable back contacts design are current interests of research. He is the author of fifty peer reviewed journals and proceedings.



**Dr. I. Saad** is an Associate Professor at the EEE Program, Faculty of Engineering, Universiti Malaysia Sabah (UMS). He received his Ph.D. from Universiti Teknologi Malaysia (UTM) and he awarded the Chancellor best student awards. His research area covers Micro and Nanoelectronics device and materials, CMOS Circuit and Nanofiber membrane for energy applications. He has secured over a million research grants with numerous dedicated collaborative research partners. He has published more than 100 Scopus index papers as primary and corresponding authors. He is now Dean in Faculty of Engineering, UMS



**Dr Y. Hong** received his Ph.D. in Chemical and Biochemical Engineering from Xiamen University in 2020. He has published in more than 14 peer-reviewed journal articles and conference proceedings. He has research interests in nanotechnology for catalysis and solar energy conversion. He had campaigned vigorously for biosynthesizing gold catalysts with high activity and high stability techniques for gas-phase propylene epoxidation in the presence of O<sub>2</sub> and H<sub>2</sub>, and biosynthesized bimetallic Au–Pd nanoparticles for solvent-free oxidation of benzyl alcohol.

**Dr Q.H. Xia** is a Professor in Zhejiang University. He has previously worked in the State Bureau of Aerospace, Ministry of Aeronautics and Astronautics Industry in Beijing, responsible for aircraft control system development.



**Dr. P. Gao** received Ph.D. degrees in Department of Physics from Lanzhou University in 2010. From 2007–2011, he worked in Nanyang Technological University as a visiting researcher and a research staff. In 2013, he joined Ningbo Institute of Materials Technology and Engineering, CAS, as an associate professor and then a professor (2015). He joined Sun Yat-sen University in 2018. His research focus on high efficiency solar cell technology, especially on developing new materials and processes for solar energy conversion. He has published over 120 journal papers and serves as an active referee for 20 journals.



**Dr. J. Ye** received the B. S. degree in Materials Science and Engineering from University of Science and Technology of China in 2001 and the Ph.D. degree in Materials Science from University of California, Davis, USA in 2005. He joined Ningbo Institute of Material Technology and Engineering, CAS, as a professor and Ph.D. advisor since August of 2012. He was awarded for "Thousand Young Talents Program of China" in 2012. He has published more than 60 publications with nearly 500 times citations, applied more than 40 patents (including 10 awarded patents).



**Dr. Z.J. Ding** received a Ph.D. from Osaka University under supervision of Prof. R. Shimizu in 1990. He then rejoined the University of Science and Technology as lecturer in 1990 and became professor of physics in Department of Astronomy and Applied Physics in 1996. He is now the group leader of Laboratory of Microstructure of Solids, and also the principle investigator of Theory and Computation Division, Hefei National Laboratory of Physical Sciences at the Microscale. His research interest is mainly on the theoretical modeling and the computation for materials characterization by surface analysis and microbeam analysis techniques.